

# 华中科技大学

## 本科毕业设计（论文）参考文献译文本

译文出处：Wang R, Herman P, Ekeberg Ö, et al. Neural and non-neural related properties in the spastic wrist flexors: an optimization study[J]. Medical Engineering & Physics, 2017, 47: 198-209.

院 系\_\_\_\_\_人工智能与自动化学院\_\_\_\_\_

专业班级\_\_\_\_\_自动化卓越 2001 班\_\_\_\_\_

姓 名\_\_\_\_\_孙徐舟\_\_\_\_\_

学 号\_\_\_\_\_U202014916\_\_\_\_\_

指导教师\_\_\_\_\_黄剑\_\_\_\_\_

2024 年 1 月 19 日

## 译文要求

- 一、译文内容须与课题（或专业内容）联系，并需在封面注明详细出处。
- 二、出处格式为  
图书：作者. 书名. 版本（第×版）. 译者. 出版地：出版者，出版年. 起页～止页  
期刊：作者. 文章名称. 期刊名称，年号，卷号（期号）：起页～止页
- 三、译文不少于 5000 汉字（或 2 万印刷符）。
- 四、翻译内容用五号宋体字编辑，采用 A4 号纸双面打印，封面与封底采用浅蓝色封面纸（卡纸）打印。要求内容明确，语句通顺。
- 五、译文及其相应参考文献一起装订，顺序依次为封面、译文、文献。
- 六、翻译应在第七学期完成。

## 译文评阅

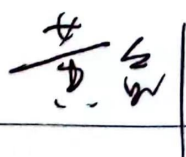
### 导师评语

应根据学校“译文要求”，对学生译文翻译的准确性、翻译数量以及译文的文字表述情况等做具体的评价后，再评分。

孙徐舟同学的毕业设计翻译紧扣研究课题，语法翻译准确、文字表达通顺，翻译字数达到学校规定的要求，是一篇合格的参考文献译文。

评分：93（百分制）

指导教师(签名):



2024 年 1 月 20 日

# 痉挛性腕屈肌的神经和非神经相关特性：优化研究

## 摘要

量化神经和非神经对痉挛性关节阻力增加的贡献对于更好地理解其病理生理机制和评估不同的干预策略至关重要。然而，直接测量痉挛相关表现，例如人类的运动神经元和生物物理特性，是极具挑战性的。在这方面，我们开发了一个前向神经肌肉骨骼模型，该模型考虑了肌梭、运动神经元池、肌肉激活和手腕屈肌肌腱的动力学，并将关节角度和阻力矩作为唯一的输入测量变量。通过模拟拉伸反射通路，在手腕伸展测试期间估计痉挛性手腕屈肌的神经和非神经相关特性。在被动腕关节伸展测试中，使用 NeuroFlexor（一种电动力测量设备）从 17 名慢性中风患者和健康对照组中收集关节角度和阻力扭矩。通过调整被动和拉伸反射相关参数来优化模型，以适应每个参与者的测量扭矩。我们发现，中度和重度痉挛患者的僵硬程度明显高于对照组。在中风幸存者的亚组中，神经成分的增加主要是由于 50% 的运动神经元募集时肌梭率较低。在所有亚组中，运动神经元池阈值与运动神经元池增益高度相关。该模型可以描述测试过程中腕关节的整体阻力行为。与对照组相比，抗性增加主要是由于较高的弹性和神经成分。我们得出的结论是，结合 NeuroFlexor 测量，所提出的神经肌肉骨骼模型和优化方案可作为研究痉挛患者拉伸反射通路潜在参数变化的合适工具。

## 1. 背景

痉挛是一种运动障碍，常见于许多神经系统疾病。它在临床上被定义为张力性拉伸反射的速度依赖性增加，并伴有过度的肌腱抽搐，这是由拉伸反射的过度兴奋性引起的[1]。在目前的实践中，痉挛通常是通过旋转关节并根据有序量表估计阻力来主观测量的，如改良的 Ashworth 评分（MAS）[2]。先前的报告表明，肌肉和肌腱的固有力学性能也可能因痉挛而发生改变，从而也可能导致关节阻力增加[3, 4]。因此，MAS 的有限可靠性和再现性，以及无法区分下方神经贡献（拉伸反射）和非神经贡献，促使开发了客观量化阻力关节扭矩的替代方法[5-7]。几个实验室已经开发了定制的仪器，以根据潜在的神经和机械特性来检查关节刚度，主要是在踝关节[8-10]和肘关节[1, 12]。最近，Lindberg 等人开发了一种机械设备，作为 MAS 测试的仪器版本，用于量化休息时手腕屈肌的痉挛。该测试也便于日常临床实践[13]。NeuroFlexor 仪器（Aggero MedTech AB，瑞典索尔纳）以两种不同的恒定速度被动地伸展手腕。力传感器测量整个运动过程中的阻力。NeuroFlexor 实时分析方法（NF 方法）[13] 可以将测量阻力扭矩的贡献分为被动弹性扭矩、被动粘性扭矩和反射扭矩（见补充文件 A）。NF 方法在慢性中风患者中得到了验证，并在神经传导阻滞测试期间，在受试者和每个受试者的肌电图（EMG）中显示了神经成分与桡侧腕屈肌（FCR）活动之间的强相关性[13]。最

近的研究还表明，NF 方法是可靠的[14]，并且足够灵敏，可以检测中风患者肉毒杆菌毒素治疗后痉挛的变化[15]。

已经提出了几种理论来解释痉挛的原因，包括拉伸反射的阈值降低或增益增加、 $\alpha$  运动神经元的过度兴奋性和肌梭的超敏[16-18]。尽管几十年的神经生理学研究丰富了我们对于痉挛的理解，但报道的数据有时是矛盾的[19]。总的来说，痉挛的病理生理机制仍然是一个有争议的问题，并且不可能直接测量人类的运动神经元和生物物理特性[20]。因此，研究人员试图开发生物力学和理论模型，以促进痉挛机制的研究。模型的复杂性各不相同，并且依赖于不同的实验协议。Koo 和 Mak[21]开发了一种神经肌肉-外骨骼模型，以模拟在肘关节以恒定角速度伸展时诱发的拉伸反射反应。他们分析了模型参数，如运动神经元池阈值和增益对肘关节生物力学行为的影响。该结果基于一名仅轻度痉挛的偏瘫受试者。De Vlugt 等人[22]通过结合机动评估和肌电图的非线性模型量化了踝关节的粘度、刚度和反射力矩。他们发现，中风患者和对照组在弹性和粘度方面存在显著差异。他们还开发了一种综合评估方案，包括被动、主动和反射测试，以测量中风后手腕运动障碍的神经和非神经因素[23]。然而，运动神经元池或肌梭行为不能被研究。Kim 等人[24]提出了一个模型，将拉伸反射系统表征为速度反馈回路，并可以识别膝关节的痉挛和内在特性。这项研究基于摆锤试验，该试验通常仅适用于膝关节肌肉痉挛。

我们的目标是建立一个包含腕屈肌拉伸反射环的前向神经肌肉骨骼模型，并证明所提出的建模和优化框架的可行性，以研究痉挛的潜在病理生理机制。该模型考虑了手腕屈肌的肌肉肌腱、肌梭和运动神经元池的适当关系。优化只需要测量的关节角度和阻力扭矩作为输入变量。所提出的计算方法可以在中风参与者和健康对照的大样本上得到广泛验证。因此，我们建模工作的主要目标是（1）检查模型识别的与拉伸反射和肌肉力学相关的成分，以及从 NF 方法获得的对应成分的相关性，以及（2）根据不同严重程度痉挛的中风患者的运动神经元池和肌梭行为的变化来确定潜在的痉挛相关表现。

## 2. 方法

### 2.1 主题

从先前的研究中选择了 17 名慢性中风（ST）患者（平均值 $\pm$ SD，年龄：50 $\pm$ 11 岁，体重：79 $\pm$ 10 kg）的样本，其中收集了 NeuroFlexor 的数据[14, 15]（表 1）。共选择 17 名没有任何神经系统疾病史的健康人（年龄：48 $\pm$ 10 岁，体重：79 $\pm$ 12 公斤）作为对照。由于 ST 段的异质性，根据 NF 方法确定的神经成分（NC），将其进一步分为三个亚组，即痉

挛程度较低的参与者（STL， $NC \leq 10N$ ）；中度痉挛（STM， $10N < NC < 30N$ ）；严重痉挛（STH， $NC \geq 30N$ ）。另外五名同时具有 FCR NeuroFlexor 和 EMG 记录的中风参与者被选为验证组。

## 2.2 实验设置和协议

使用 NeuroFlexor 测量阻力扭矩，这是一种便携式计算机控制的伺服电机系统，包括一个高分辨率步进电机和一个电机控制器，可在慢速（ $5^\circ \text{ s}^{-1}$ ）和快速（ $236^\circ \text{ s}^{-2}$ ）速度下产生恒定运动（详见[13]和补充文件 B）。所有参与者的手腕运动范围设定为从  $20^\circ$  屈曲到  $30^\circ$  伸展。对于验证组中的另外 5 名参与者，从 FCR (MYO 15, Liberty Technology, Hopkinton, Massachusetts) 记录表面肌电。为了避免噪声放大，对原始扭矩和角度数据进行低通滤波，截止频率为 10 Hz（二阶巴特沃斯滤波器）。根据赫尔辛基宣言，所有参与者均给予书面知情同意书。这项研究得到了瑞典斯德哥尔摩卡罗琳斯卡研究所区域伦理委员会的批准。

## 2.3 神经肌肉骨骼模型

我们的神经肌肉骨骼模型包括描述肌肉肌腱、肌梭、运动池和手腕屈肌肌肉激活动力学的组件（图 2-1）。

### 2.3.1 肌腱模型

肌肉肌腱模型由一个代表协同手腕屈肌的集中肌肉致动器和一个被动单元组成[25]。腕伸肌不包括在模型中，因为它们在被动腕伸展运动过程中的激活可以忽略不计。

运动方程：根据被动伸腕运动过程中的动态平衡确定建模的手腕阻力扭矩：

$$T_m = (J_h + J_{hp})\ddot{\theta} + T_{MA} + T_{PP} + T_{Gh} + T_{Ghp} \quad (2-1)$$

其中， $T_m$  为模型阻力矩， $J_h$  和  $J_{hp}$  为手段和手板的惯性矩， $\ddot{\theta}$  为角加速度， $T_{MA}$  为集中肌肉致动器产生的扭矩， $T_{PP}$  为被动单元产生的扭矩； $T_{Gh}$  和  $T_{Ghp}$  分别为手段与手板重力产生的扭矩，

$$J_h = m_h(K_{cg}I_h)^2 + m_h(K_{proximal}l_h)^2 \quad (2-2)$$

根据手部的质量（ $m_h$ ）和长度（ $I_h$ ）以及回转半径长度与手部绕重心（ $K_{cg}$ ）和近端关节（ $K_{proximal}$ ）的长度的比例来估计手部的惯性矩[26]。使用初始阻力扭矩偏移来估计手板的惯性矩。

被动单元：模型中的被动单元被视为关节肌肉和结缔组织的被动粘弹性元件[25]：

$$T_{pp} = K_p(\theta - \theta_0) + B_p\dot{\theta} + k_1e^{k_2(\theta - \theta_0) - 1} \quad (2-3)$$

其中， $K_p$ 为刚度系数， $B_p$ 为粘性系数， $k_1$ 和 $k_2$ 为非线性指数系数， $\theta_0$ 为肌腱松弛长度处的静止关节角，因此， $T_{pp}$ 等于零。

表 2-1 参与者的临床描述（ST：中风患者，C：对照组，V：验证受试者）  
Clinical description of participants (ST: persons with stroke, C: controls, V: validation subjects).

Participants	Gender	Age (Years)	Weight (Kg)	Lesion Type	Post Stroke Time (Months)	Modified Ashworth Score
ST1	M	66	87	Ischemic	86	1
ST2	M	57	82	Ischemic	120	3
ST3	F	30	83	Trauma	111	3
ST4	F	62	60	Ischemic	114	4
ST5	M	43	77	Ischemic	37	4
ST6	M	56	96	Haemorrhagic	123	3
ST7	F	55	74	Haemorrhagic	55	4
ST8	M	45	75	Ischemic	10	0
ST9	M	47	100	Ischemic	28	3
ST10	M	44	80	Haemorrhagic	36	3
ST11	M	63	71	Ischemic	10	2
ST12	M	59	69	Ischemic	50	2
ST13	M	51	75	Haemorrhagic	12	3
ST14	M	46	84	Haemorrhagic	44	1
ST15	M	47	82	Haemorrhagic	16	4
ST16	M	61	78	Haemorrhagic	7	3
ST17	M	22	75	Haemorrhagic	20	4
C1	M	36	75	-	-	-
C2	F	38	65	-	-	-
C3	F	60	60	-	-	-
C4	F	36	75	-	-	-
C5	F	32	70	-	-	-
C6	F	32	60	-	-	-
C7	M	47	78	-	-	-
C8	M	47	85	-	-	-
C9	M	47	108	-	-	-
C10	M	49	92	-	-	-
C11	M	50	90	-	-	-
C12	M	55	82	-	-	-
C13	M	55	89	-	-	-
C14	M	55	70	-	-	-
C15	M	58	82	-	-	-
C16	M	58	80	-	-	-
C17	M	59	90	-	-	-
V1	M	40	88	Haemorrhagic	55	1+
V2	M	61	87	Haemorrhagic	75	0
V3	F	66	79	Haemorrhagic	43	3
V4	F	72	80	Ischemic	86	4
V5	F	63	69	Haemorrhagic	90	2

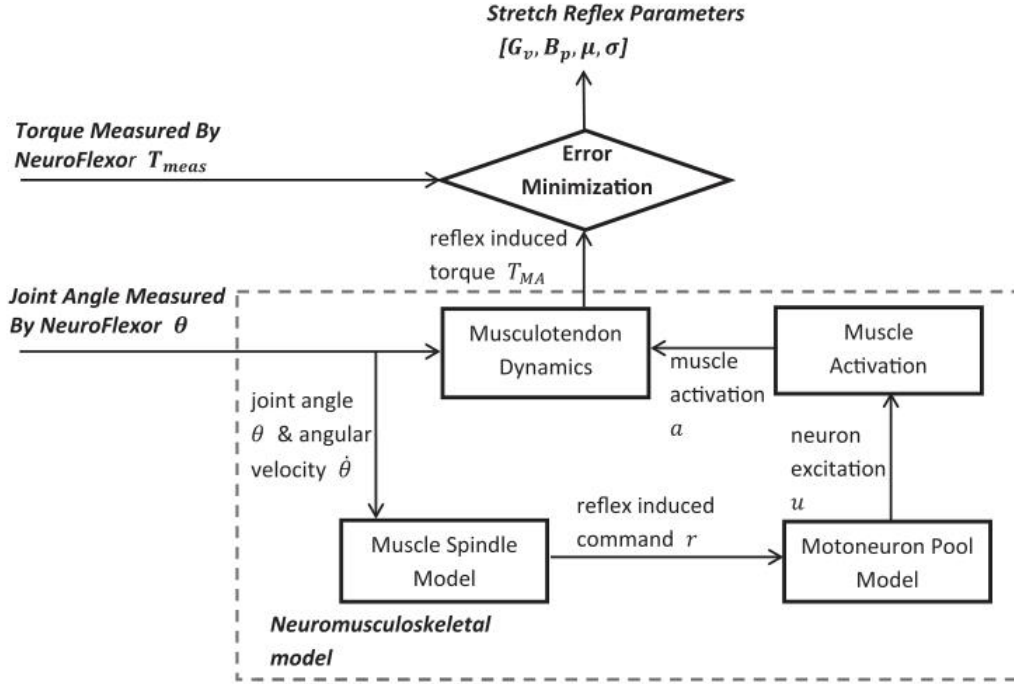


图 2-1 神经肌肉骨骼建模的示意图，用于使用优化量化被动拉伸反射参数。神经肌肉骨骼模型包括描述肌肉肌腱、肌梭、运动神经元池和手腕屈肌激活动力学的组件。

弹性分量（EC）是  $T_{pp}$  的角度相关扭矩分量，粘度分量（VC）是角速度相关扭矩分量

$$EC = K_p(\theta - \theta_0) + k_1 e^{k_2(\theta - \theta_0) - 1} \quad (2-4)$$

并且

$$VC = B_p \dot{\theta} \quad (2-5)$$

集中肌肉致动器：集中肌肉致动器被建模为与一系列弹性元件串联的收缩元件。关节力矩角和力矩角速度关系在致动器模型中实现[25]。

$$T_{MA} = a f_v(\dot{\theta}) f_l(\theta) \quad (2-6)$$

对于肌肉激活（参见肌肉激活动力学）， $f_v$  是力矩-角速度关系， $f_l$  是力矩-角度关系。在被动手腕伸展中，肌肉激活  $a$  被认为完全是由手腕屈肌的拉伸反射引起的。因此，神经成分（NC）相当于  $T_{MA}$ 。

### 2.3.2 肌梭建模

实施了改进的混合  $v^{0.6}$  模型[27]，以描述作为关节角度和角速度函数的延长过程中肌肉纺锤体的发射特性：

$$r(t) = G_v(\dot{\theta}(t - \tau_{SDR}))^{0.6} + G_l(\theta(t - \tau_{SDR}) - \theta_0) + r_0 \quad (2-6)$$

其中  $r$  为 Ia 传入（初级传入）放电速率， $\theta_0$  为静息关节角， $\tau_{SDR}$  为拉伸反射延迟， $G_v$  和  $G_l$  分别为纺锤体模型的动态和静态增益， $r_0$  为 Ia 神经元的背地放电速率。 $\tau_{SDR}$  和  $r_0$  设置为  $30\text{ ms}$  和  $6.45\text{ imps}^{-1}$  [28]。

### 2.3.3 运动神经元池建模

$\alpha$ -运动神经元池的输入-输出关系由高斯累积分布函数表示[29]。如前所述[21]，我们还假设，除了来自肌梭的突触输入外，所有进入  $\alpha$ -运动神经元池的突触输入都可以被视为被动运动中的常数，并且由肌梭引发的突触电流与肌梭放电率成线性比例。因此，运动神经元池转化，代表运动神经元兴奋作为肌梭发射率的函数，被建模为范围从 0 到 1 的 S 形函数，

$$u(t) = \frac{1}{1 + e^{\frac{\mu - r(t)}{\sigma}}} \quad (2-7)$$

$u$  为运动神经元池的神经兴奋， $\mu$  为 50% 运动神经元募集时的纺锤体放电率， $\sigma$  为累积分布函数的标准偏差。

为了更好地解释和更有生理意义，根据先前研究的定义，进一步计算了手腕屈肌运动神经元池的阈值和增益[21]。阈值  $\mu_0$  对应于导致 0.005 神经兴奋的主轴点火率，增益  $G_0$  定义为：

$$G_0 = \frac{0.6}{r_{0.8} - r_{0.2}} \quad (2-8)$$

当  $r_{0.8}$  和  $r_{0.2}$  时，80% 和 20% 运动神经元完全恢复时的肌梭放电率。

### 2.3.4 肌肉激活动力学

激活动力学被描述为将神经兴奋  $u(t)$  转化为肌肉激活  $a(t)$  的过程，作为一阶微分方程[30]：

$$\dot{a}(t) = \frac{u(t) - a(t)}{\tau(a(t), u(t))} \quad (2-9)$$

$$\tau(a(t), u(t)) = \begin{cases} \tau_{act} (1.5a(t) + 0.5)u(t) > a(t) \\ \tau_{dact} / (1.5a(t) + 0.5)u(t) \leq a(t) \end{cases} \quad (2-10)$$



$\tau$  是随着激活水平和肌肉激活水平的动态变化（增加或减少）而变化的时间常数， $\tau_{act}$  和  $\tau_{dact}$  是激活和失活的时间常数。

## 2.4 最优化

模型中的每个参与者都需要调整四个被动关节参数 [ $K_p$ ,  $B_p$ ,  $k_1$ ,  $k_2$ ] 和四个拉伸反射相关参数 [ $G_v$ ,  $G_l$ ,  $\mu$ ,  $\sigma$ ]。

### 2.4.1 被动参数

据推测，在缓慢运动过程中，拉伸反射引起的肌肉阻力可以忽略不计；因此，阻力扭矩完全由被动单元引起。基于慢速运动中阻力扭矩的实验测量，使用非线性最小二乘法（NLS）优化来近似被动参数。这些参数的初始值从文献[25]中获得： $K_p=1 \text{ Nm/rad}$ ,  $B_p=0.1 \text{ Nms/rad}$ ,  $k_1=0.37 \text{ Nm}$ ,  $k_2=3.44 \text{ rad}^{-1}$ 。为了避免测量的加速和减速阶段，从分析中省略了缓慢移动的最初 0.5 s 和最后 2 s。假设在快速运动的第一个峰值处拉伸反射诱导的扭矩可忽略不计，通过最小化建模的阻力扭矩和测量的阻力扭矩之间的差异来进一步校正粘度系数  $B_p$ （PI，图 4）。

### 2.4.2 拉伸反射相关参数

遗传算法（GA）[31]用于通过最小化快速运动中测量和建模的阻力扭矩之间的均方根误差（RMSE）来确定最佳拉伸反射相关参数。遗传算法是一种基于模仿生物进化的自然选择概念的优化方法。本研究中的遗传算法配置有双精度浮点表示、高斯分布的加性突变、单点交叉和随机一致选择[31]。对来自 ST 组的 10 名随机选择的参与者进行了试点敏感性分析，以确定 GA 的基本参数：群体规模（50）、交叉（0.8）和突变率（0.1）以及收敛的最大生成次数（100）。为了获得可靠的最佳拉伸反射相关参数，从不同的初始群体开始，对每个参与者的每个个体试验重复 GA 10 次。最终选择的参数对应于找到的最佳解决方案，即具有最小 RMSE 的解决方案。

在适应度函数（上述 RMSE）的计算中，设备偏移被包括在预测的阻力矩中，该阻力矩被定义为在快速运动过程中没有手的情况下建模的阻力矩和测量的阻力矩之间的差异。由于病理组的肌梭静态和动态增益与健康对照组相似[32]，因此对  $G_v$  和  $G_l$  施加了限制，使其与报告值（分别为 4.3 和 2.0）相差  $\pm 10\%$ 。

## 2.5 数据分析和统计

从每个参与者的 Neu-roFlexor 测量中选择一组具有代表性的试验（一个慢动作、一个快动作、一次无手慢动作和一次无手快动作），通过 NF 方法和优化计算 EC、VC 和 NC。同样的试验也用于使用神经肌肉骨骼模型和优化计算被动和拉伸反射相关参数。原始 EMG 数据以 1000Hz 采样，整流并线性包络（截止频率为 6 Hz 的二阶双向巴特沃斯滤波器）[33]。

每次试验的模型有效性由方差分析（VAF）和决定系数（ $R^2$ ）确定，它们描述了模拟和测量的阻力扭矩的“拟合优度”[22]：

$$VAF = (1 - \frac{\sum \epsilon(t)^2}{\sum T_{means}(t)^2}) \cdot 100\% \quad (2-11)$$

$$R^2 = 1 - \frac{\sum \epsilon(t)^2}{\sum (T_{means}(t) - \bar{T}_{means})^2} \quad (2-12)$$

$\epsilon(t)$  是误差，即在  $t=1, \dots, N$  个样本上测量的阻力扭矩  $T_{means}(t)$  和模型阻力扭矩  $T_m(t)$  之间的差， $\bar{T}_{means}$  是测量阻力扭矩的平均值。

为了验证模型拟合的泛化方面，还使用从优化中获得的被动和拉伸反射相关参数，在每个参与者的三组额外的测量试验中确定了 VAF。我们还通过计算敏感性指数（SI）来检查模型对被动和拉伸反射相关参数的敏感性，如补充文件 C 中详细讨论的那样。

描述性统计以中位数和范围表示。在整个研究中使用了非参数统计检验。采用 Spearman 秩序相关检验，分别研究了 NF 方法和优化方法识别的成分之间的相关性。为了检验组间差异，使用 Mann-Whiney U 检验。为了测试 HC 组和中风参与者亚组之间的反射和拉伸反射相关参数的差异，使用了 Kruskal-Wallis H 检验。如果综合检验显著，则应用与 Bonferroni 调整的事后配对比较。

### 3.结果

#### 3.1 被动参数

在缓慢运动过程中，当手腕从初始位置被动伸出时，总阻力矩呈线性增加，当关节向最大测量角度伸出时，阻力矩呈指数级略有增加。例如，图 2（B）显示了一名中风参与者和一名健康对照者在缓慢运动过程中建模和测量的总阻力矩。它说明了模型的良好拟合，并在所有参与者中观察到一致的结果（表 2）。额外试验

集的 VAF 值与用于优化的三值相似（ST:99.2%±1.8%，Control:99.4%±1.5%），这验证了模型适用于个体参与者的泛化特性。

与对照组相比，中风参与者的刚度系数  $K_p$ （ $p<0.01$ ）和非线性系数  $k_1$ （ $p=0.031$ ）显著较高。进一步的亚组比较显示，STL 组的  $K_p$  和  $k_1$  与对照组相似，但 STM 和 STH 组的  $K_p$  和  $k_1$  明显高于对照组（图第 3 和表 3）。

表 3-1 在慢速和快速运动过程中，模型扭矩和测量扭矩之间的方差（VAF）和决定系数（ $R^2$ ）

The Variance Accounted For (VAF) and the coefficient of determinations ( $R^2$ ) between modeled and measured resistant torque during the slow and fast movement.

Mean (S.D)	Slow movement		Fast movement	
	VAF	$R^2$	VAF	$R^2$
Control	98.12% (2.11%)	0.99 (0.002)	N/A	
ST	98.62% (2.30%)	0.99 (0.003)	98.23% <sup>a</sup> (1.39%)	0.89 (0.04)

<sup>a</sup> The average VAF value was calculated when two outliers in the STL group were excluded.

3.2 拉伸反射相关参数

由于 0.05–0.09 s 记录期间的测量误差和反射延迟，仅对快速运动的选定部分进行了优化(从测量的总阻力扭矩的第二个峰值 PII 到第三个峰值 PIII, 图 3-3(B))，在此期间角速度保持稳定（图 3-3（a））。拉伸反射相关参数仅在 ST 组中确定。例如，图 3-3（B）显示了一名参与者在快速运动过程中中风时的阻力矩模型和测量结果。它还说明了模型与数据的良好拟合。除了 STL 组中的两个异常值外，在所有参与者中都观察到了一致的结果（表 3-1）。额外试验组的 VAF 值与用于优化的试验相似（95.4%±3.5%）。此外，如一名患者的例子所示，FCR 的开始时间与验证组中建模的估计肌肉活动时间一致（图 3-4）。

在中风幸存者组中，两个运动神经元池参数（ $\mu$ 和 $\sigma$ ）显示出随着痉挛程度的增加而下降的趋势（表 3-2）。轻度和重度感染组之间的 $\mu$ 有显著差异（ $p=0.01$ ），但 $\sigma$ 无显著差异。

痉挛更严重的参与者运动神经元池阈值  $\mu_0$  略低，增益  $G_0$  较高，但差异不显著。

在所有三个亚组中， $\mu_0$  和  $G_0$  之间均具有显著且非常高的相关性（STL: $p<0.01$ ， $r=0.99$ ，STM: $p<0.01$ 、 $r=0.90$ ，STH: $p<0.01$  和  $r=0.96$ ，图 6 和图 7）。

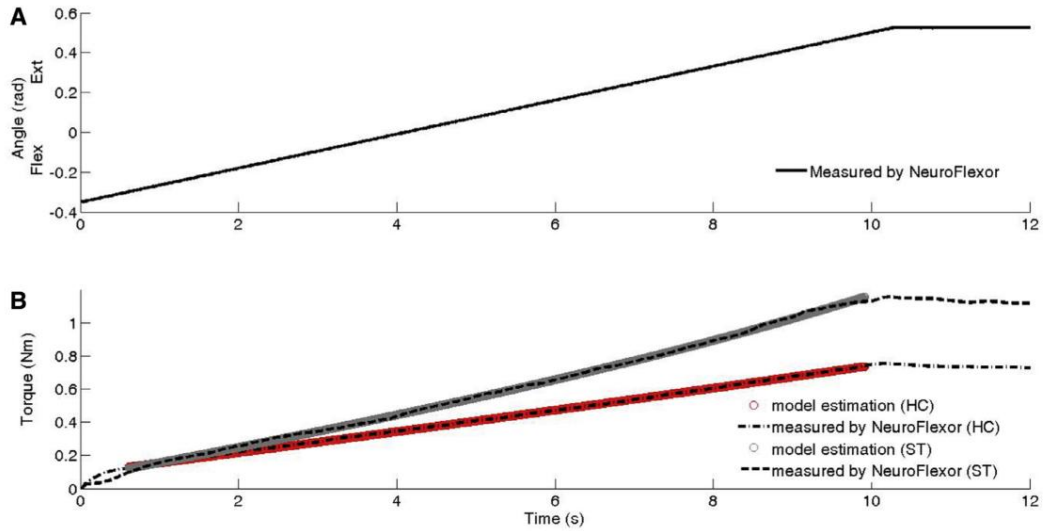


图 3-1 (A) 在缓慢运动中，使用 NeuroFlexor 以 5°/s 的速度被动地将腕关节从 20°（0.35 rad）延伸到 30°（0.52 rad）。(B) 通过拟合慢运动中测量的扭矩，使用非线性最小二乘优化来预测被动参数。黑色虚线和点划线分别表示代表性健康受试者和中风患者的测量阻力矩。带有灰色和红色圆圈的线表示相同受试者的建模阻力扭矩。

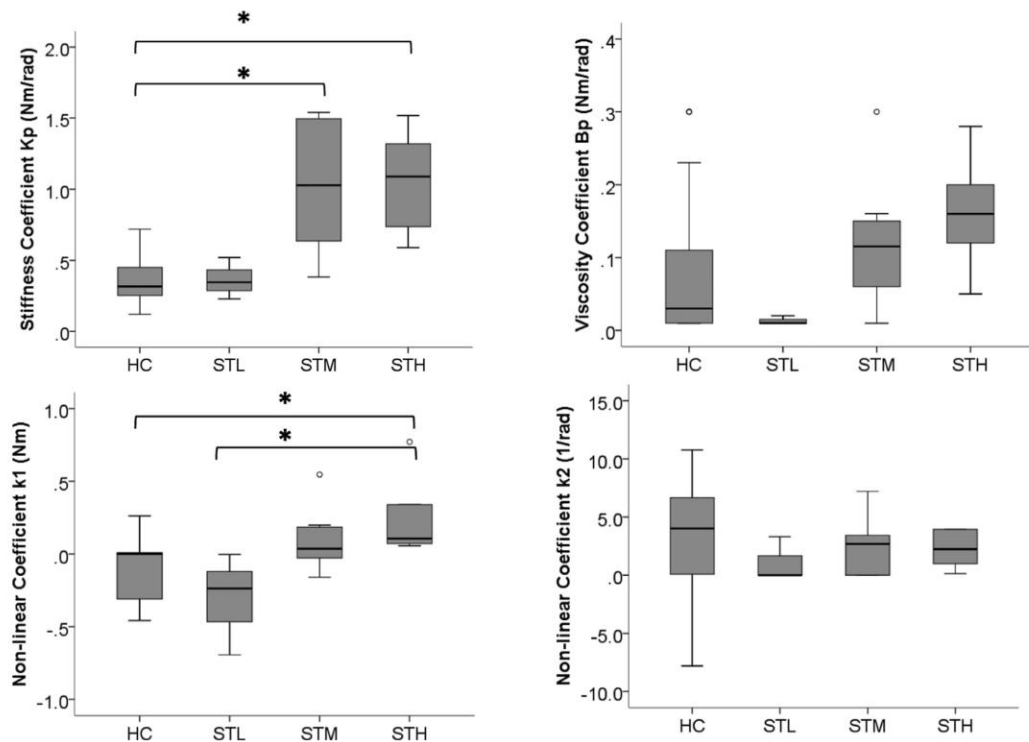


图 3-2 在对照组（HC）和轻度（STL）、中度（STM）和重度（STH）痉挛的卒中组中，估计的刚度系数  $K_p$ 、粘度系数  $B_p$  和两个非线性系数  $k_1$  和  $k_2$  作为方框图。星号表示各组之间的显著差异。空心圆表示大纲视图。

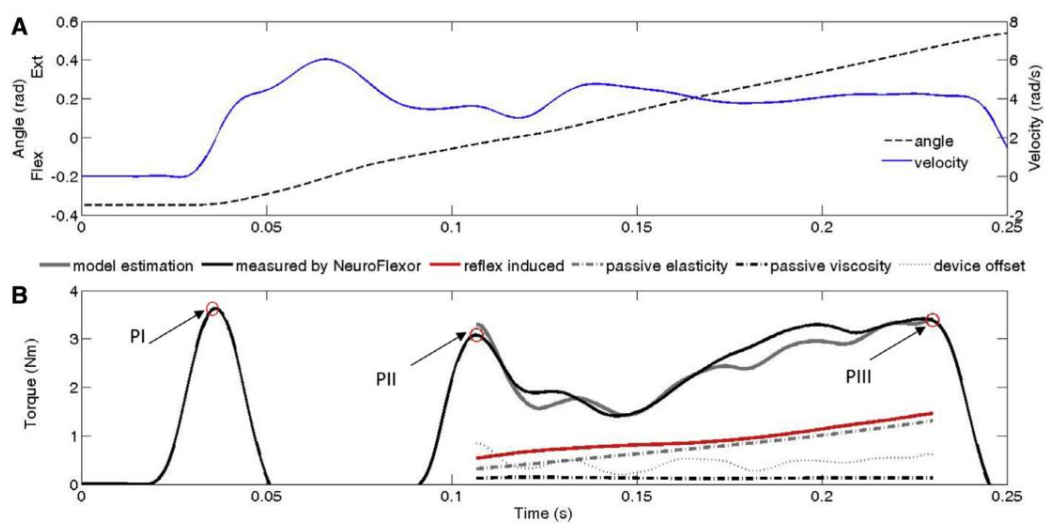


图 3-3 (A) 在快速运动中，使用 NeuroFlexor 以  $236^\circ/\text{s}$  ( $4.08 \text{ rad/s}$ ) 的速度将腕关节从  $20^\circ$  ( $0.35 \text{ rad}$ ) 的屈曲被动地伸展到  $30^\circ$  ( $0.52 \text{ rad}$ )。黑色虚线和黑色实线分别表示测得的关节角和角速度。(B) 使用遗传算法 (GA) 来估计拉伸反射

相关参数。通过最小化 PI 下的建模阻力扭矩和测量阻力扭矩之间的差异来校正从缓慢运动估计的粘度系数  $B_p$ 。优化仅用于匹配 PII 与 PIII 期间记录的数据。指定了被动（弹性、粘度）和拉伸反射反射参数对阻力扭矩的贡献

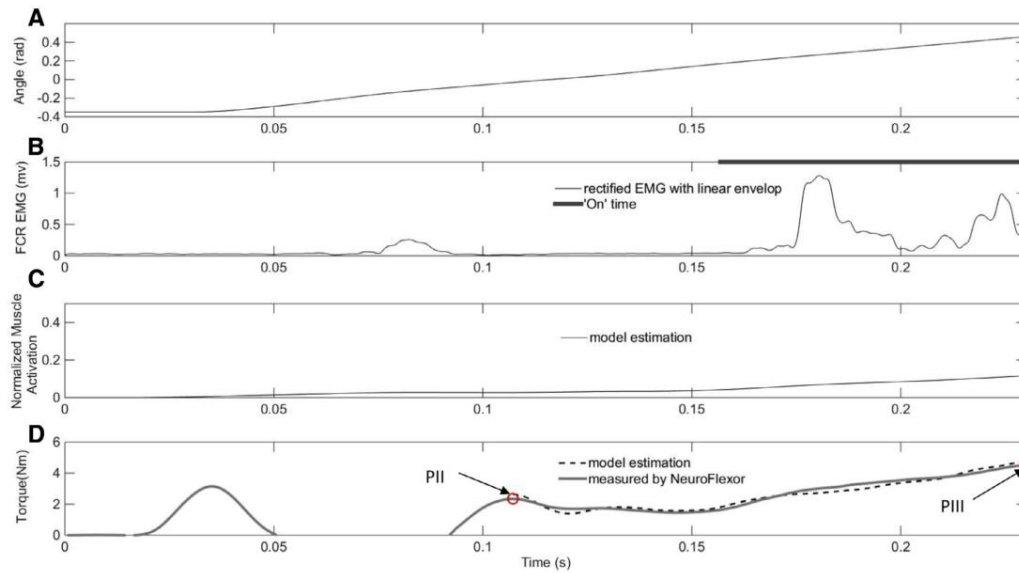


图 3-4 (A) 在快速运动中，使用 NeuroFlexor 将腕关节从  $20^\circ$  (0.35 弧度) 的屈曲被动延伸到  $30^\circ$  (0.52 弧度) 的伸展。(B) 原始 EMG 记录在 800Hz 下采样，整流并以 6Hz 的截止频率线性包络。FCR 被定义为当 EMG 信号高于阈值时激活，该阈值是基线 EMG 的三倍 SD。粗灰线表示在 PII 至 PIII 期间确定的 FCR 的活动开始。(C) 模型估计了快速运动中手腕伸展引起的肌肉激活。(D) 在 PII 至 PIII 期间，建模和测量的阻力手腕扭矩显示出良好的拟合性

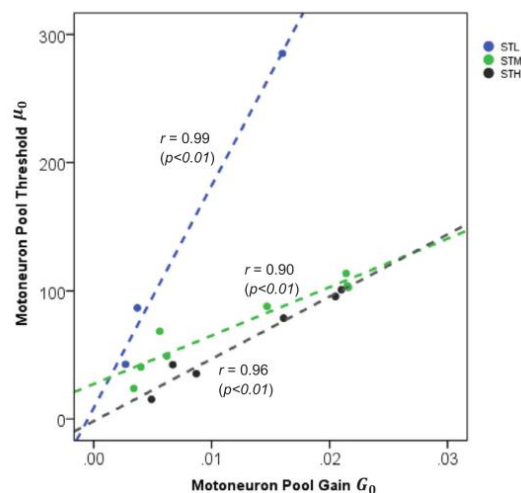


图 3-5 在对照组（HC）、轻度受累组（STL）、中度受累组（STM）和重度受累组（STH）中测定了高度相关的运动神经元池阈值  $\mu_0$  和增益  $G_0$  参数。虚线表示数据的线性回归拟合。

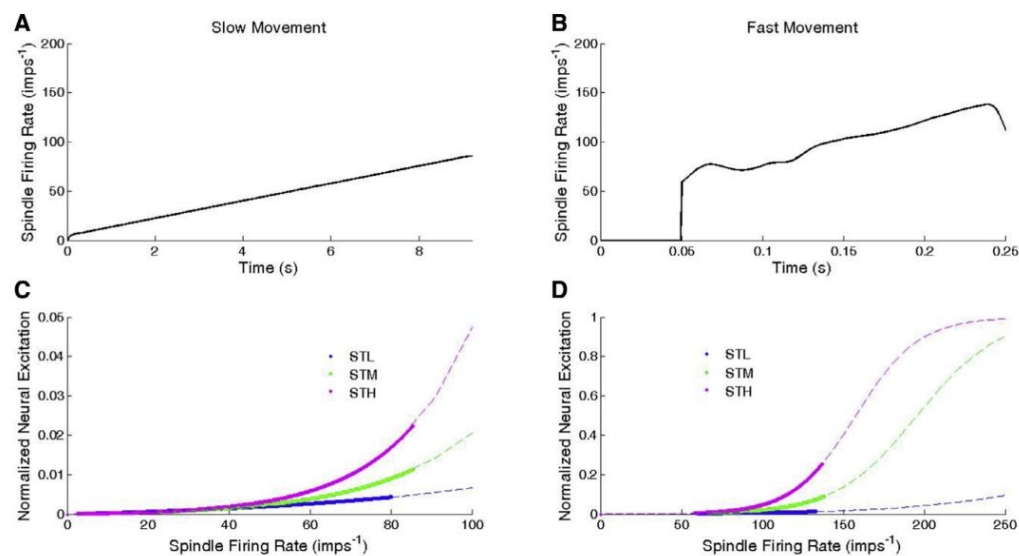


图 3-6（A）–（B）模型估计了在慢速和快速运动中手腕伸展引起的肌梭放电率。（C）–（D）在轻度受影响（STL）、中度受影响（STM）和个别受影响组（STH）中，使用优化方法估计平均运动神经元池分布。品红色、绿色和蓝色的虚线表示整个纺锤体发射率范围（0-250 imps<sup>-1</sup>）内的运动神经元池轮廓，实线对应于研究中估计的神经元兴奋范围。

表 3-2 每组的被动和反射相关参数（中位数和范围），中风组和对照组之间的显著差异用粗体显示。显著的亚组差异用粗体斜体表示

**Table 3**  
The passive and reflex related parameters (median and range) in each group. Significant differences between stroke and control groups were illustrated in bold. Significant subgroup differences were illustrated in bold italic.

Median (Min, Max)	Passive parameters				Reflex related parameters					
	$K_p$ (Nm rad <sup>-1</sup> )	$B_p$ (Nms rad <sup>-1</sup> )	$k_1$ (rad <sup>-1</sup> )	$k_2$ (rad <sup>-1</sup> )	$G_1$	$G_0$	$\mu$	$\sigma$	$\mu_0$	$G_0$
<b>Control</b>	0.32 (0.12, 0.72)	0.03 (0.01, 0.30)	0.001 (-1.98, 0.26)	4.01 (-7.81, 10.77)	N/A					
<b>ST</b>	<b>0.86</b> <b>(0.23, 1.54)</b>	0.12 (0.01, 0.33)	<b>0.05</b> <b>(-0.69, 0.37)</b>	2.14 (-0.004, 7.23)						
<b>STL</b>	0.35 (0.23, 0.52)	0.01 (0.01, 0.02)	-0.24 (-0.69, -0.004)	0.003 (-0.0001, 3.31)	1.94 (1.91, 2.09)	4.33 (4.18, 4.39)	<b>379.30</b> <b>(356.68, 390.31)</b>	58.10 (13.52, 79.16)	86.72 (42.72, 285.12)	0.005 (0.003, 0.016)
<b>STM</b>	<b>1.03</b> <b>(0.38, 1.54)</b>	0.12 (0.10, 0.33)	0.04 (-0.16, 0.55)	2.69 (-0.004, 7.23)	2.07 (2.00, 2.09)	4.21 (4.08, 4.80)	195.65 (155.73, 289.50)	24.80 (10.00, 62.75)	78.21 (23.92, 113.67)	0.01 (0.003, 0.021)
<b>STH</b>	<b>1.15</b> <b>(0.15, 1.53)</b>	0.16 (0.20, 0.28)	0.11 (0.03, 0.37)	0.99 (0.13, 3.94)	2.08 (2.00, 2.09)	4.12 (4.10, 4.49)	<b>157.62</b> <b>(150.03, 203.70)</b>	19.15 (10.29, 32.44)	60.56 (15.36, 100.88)	0.012 (0.005, 0.02)

### 3.3 来自模型估计和 NF 方法的单个分量的相关性

在快速移动中阻力扭矩的第三个峰值处，在中风幸存者组中识别出 EC、VC 和 NC（PIII，图 4（B）），与 NF 方法相同。根据当前模型估计计算的单个分量与基于 NF 方法的分量非常相关（图 8）。在 NC 中确定了显著且非常高的相关性（ $p<0.01$ ， $r=0.94$ ），在 EC 中确定了高相关性（ $p<0.01$ ， $r=0.84$ ），而在 VC 中确定了中等相关性（ $p<0.01$ ， $r=0.70$ ）。

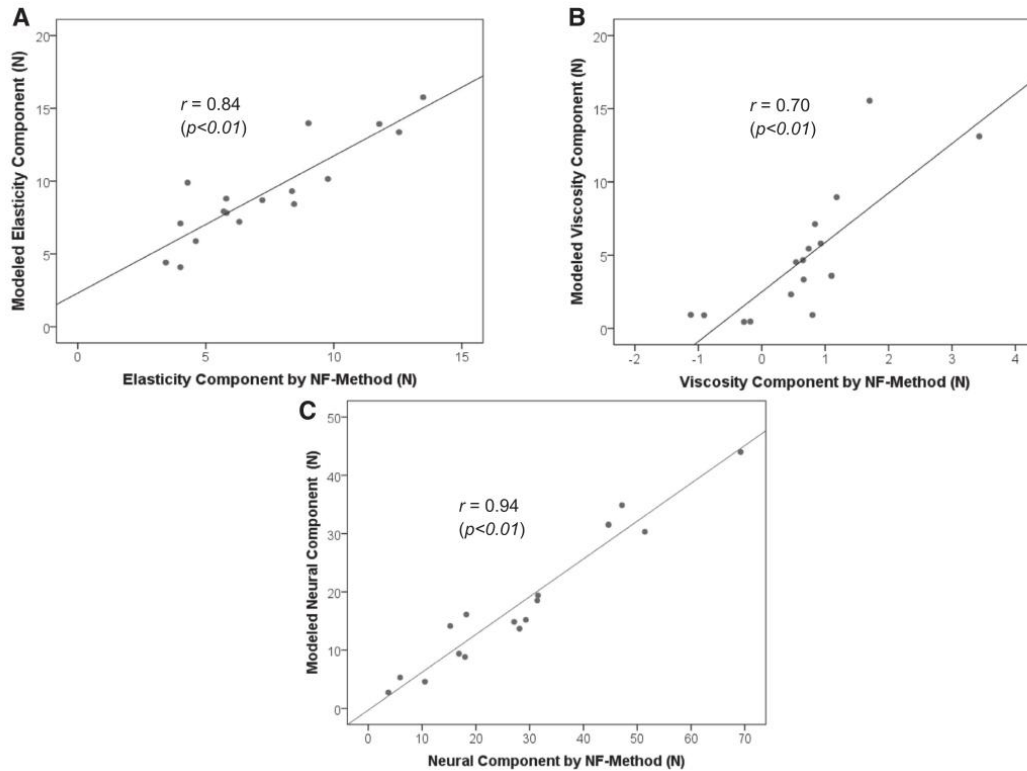


图 3-7 在患者组中，通过 NF 方法估计的成分与模型估计（A）弹性成分、EC（B）粘度成分 VC 和（C）神经成分 NC 之间的相关性。这些线表示与数据的线性回归拟合。

#### 4.讨论

我们建立了一个神经肌肉骨骼模型来模拟痉挛的被动手腕伸展测试。通过明确建模肌肉肌腱、肌梭和运动神经元池参数，使用优化技术估计了慢性中风患者腕关节的神经和非神经相关特性。与对照组相比，中风幸存者表现出更高的被动僵硬。运动神经元池参数往往随着痉挛程度的增加而减少。此外，运动神经元池阈值和增益在所有三个子组中都高度相关。



据我们所知，这是第一项试图通过结合运动测量和神经肌肉骨骼建模来研究手腕肌肉痉挛潜在潜在潜在机制的研究，关节角度和阻力扭矩是唯一的输入测量变量。

#### 4.1 方法的有效性

神经肌肉骨骼模型首次使用 VAF 进行验证。对于慢速和快速运动，所有参与者的 VAF 值均高于 90%（STL 组中的两个异常值除外）。我们还发现，建模的阻力扭矩和测量的阻力扭矩之间存在非常高的相关性（表 2）。VAF 的高值和确定的协同效应表明，整个模型经过了全面优化，可以对当前测试条件下的总阻力转矩做出可靠的预测。据报道，健康人的被动手腕硬度和粘度范围为 0.32–0.41  $Nm/rad$  和 0.02–0.04  $Nm/rad$  [34, 35]。文献中没有发现中风幸存者的可比较数据。由于测试条件和建模方法的不同，不适合与其他结果直接比较。然而，当前研究中的模型刚度和粘度在报告值的范围内。

与大多数其他使用肌电图记录直接量化神经对关节阻力的贡献的研究不同[8, 9, 22, 36]，拉伸反射特性是通过明确建模肌梭和运动神经元池来估计的。为了验证，我们将另外五名参与者纳入了 FCR 的肌电图记录。模型估计肌肉活动的时间与记录的 EMG 反应一致（图 5）。所提出的方法的好处是不需要 EMG 记录，这使我们的方法在日常临床实践中更加实用和有用。更重要的是，它仍然允许研究潜在的痉挛机制，因为运动神经元库的整体输入-输出关系可以量化。

通过比较给定参数的自协方差和互协方差分量，也可以通过参数的相互依赖性来深入了解参数估计的可靠性。结果揭示了有助于解释模型输出方差的参数之间的相互作用。低相互依赖性意味着参数估计是可靠的[22]。我们发现，对于所有八个参数，自协方差都高于相应的互协方差因子，这表明参数估计是可靠的。此外，与其他被动参数和与拉伸反射相关的参数相比，该模型对  $K_p$  和  $\mu$  的敏感性更高，尽管总体估计表明影响大小适中（表 S1，补充文件 C）。

#### 4.2 模型考虑因素

不管被动拉伸反射回路中涉及的神经回路的复杂性如何，反射回路的建模都得到了简化，由肌梭和运动神经元池模型组成。哺乳动物运动神经元库的输入-输出特性仍然未知，但是，从稳态条件推导的运动神经元库计算机模拟与动物实验数据显示出良好的定性一致性[29, 37]。先前的研究已经证明了纺锤体模型的简化结

构在人体肌肉纺锤体中产生生理现实行为的效用[38]。混合 V 0.6 模型的静态和动态增益反映了  $\gamma$ -运动神经元的激活水平。最近的研究表明，中风患者的肌梭放电率与对照组相似[3]。因此，我们假设肌梭的敏感性对拉伸反射的影响很小，从而对痉挛程度的影响也很小。过度活跃的拉伸反射主要是由于运动神经元池的输入输出关系异常。运动神经元池的特征参数（阈值和增益）应解释为直接或间接突触到运动神经元池上的所有兴奋性和抑制性输入的总体影响，如突触前抑制、相互抑制和  $\alpha$ -运动神经元兴奋性，类似于以前的建模方法[21]。

本研究采用集中参数肌肉肌腱模型。这种类型的模型被认为是最简单的模型，充分代表了单自由度关节运动的基本特征[39]。尽管有三种主要的手腕屈肌，但它们在纤维类型、起源和手腕屈伸的解剖功能方面是相似的[40]。我们假设集总模型可以有效地表示手腕屈肌的整体结构。

### 4.3 单个成分和与 NF 方法的比较

在 ST 组中与 NF 方法同时计算 EC、VC 和 NC（在快速运动中的最大阻力力矩下，PIII），以检查使用 NF 方法和神经肌肉骨骼模型的分量估计是否存在系统差异。在对照组和 STL 组中，EC 是总阻力扭矩的最大贡献者，其次是 NC。在 STM 和 STH 组中，NC 而不是 EC 是最大贡献者。VC 对所有参与者的贡献最小。特别是随着行程的增加，总阻力扭矩的增加主要是由于 NC 和 EC 的增加。在所有三种成分中都发现了与 NF 方法的中等到非常高的相关性，其中 NC 的相关性最高，VC 的相关性最低。VC 的中等相关性是由于两种方法中的定义不一致。视觉力取决于速度，可能与肌肉纤维滑动产生的剪切力有关[41]。因此，在该模型中，VC 被定义为与角速度线性相关的项。由于 NF 方法的性质，VC 只能在快速运动的第一个峰值（早期粘度），根据拉伸反射[13]发展之前的力迹准确计算。假设速度保持不变，PIII 的后期粘度估计为早期粘度的 20%[42]。根据我们的估计，ST 组的后期粘度为早期粘度的 70%（69–72%）。尽管需要更大样本量的进一步研究，但 NF 方法似乎低估了 VC 的贡献。

### 4.4 被动和拉伸反射相关参数

#### 4.4.1 被动参数

与对照组相比，由于线性和非线性指数项增加，STM 和 STH 组的刚度显著更高。正如预期的那样，控制具有非常小的非线性系数  $k_1$ ，因为测试 ROM 远小于它

们的最大延伸角。因此，被动组织呈现出准线性阻力扭矩，以响应手腕角度的增加。除了较高的机械肌肉刚度  $K_p$ （线性项）外，较高的非线性系数（经验项）可能表明中风幸存者的腕关节 ROM 较小。肌肉和/或结缔组织缩短组织，如在痉挛患者中经常观察到的，可能会导致僵硬力矩指数上升的较早开始。在之前的一项中风发作研究中发现了类似的观察结果，尽管对组织硬度的建模不同[43]。与我们的发现相反，NeuroFlexor 之前的一项研究报告称，只有一些中风参与者的硬度增加[13]。这种不一致可能是由于研究队列中痉挛程度不同。尽管粘度系数  $B_p$  倾向于随着痉挛程度的增加而增加，但粘度对总阻力矩的贡献通常很小，尤其是在等速测试条件下。由于文献中对粘度的定义各不相同，据报道，在上肢痉挛的中风患者中，肌肉粘度的发现不一致[13, 43]。痉挛肌粘度特性的改变被认为是由于肌肉的细胞内和细胞外基质的成分变化[44]。

#### 4.4.2 拉伸反射相关参数

通过确定每个中风幸存者的运动神经元池特征，进一步研究 NC 的增加。STL 组和 STH 组之间存在显著差异。在我们的建模和分析中，过度活跃反射主要是由于较低的  $\mu$ 。为了对每个参与者的运动神经元池轮廓进行更有意义的解释，定义了阈值  $\mu_0$ （最小纺锤体发射率）和增益  $G_0$ （中程斜率）。在生理学上， $G_0$  可以被解释为与被动膜性质和电压感应膜电导相关的内在运动神经元特性[21]。 $\mu_0$  可以解释为运动神经元池的净兴奋性和抑制性输入。理论上，反射诱导的神经兴奋可以通过减少  $\mu_0$  来增强，而不改变轮廓（ $G_0$ ）的形状，即将轮廓曲线向左移动。在中风参与者中， $\mu_0$  随着痉挛严重程度的增加而呈下降趋势，而  $G_0$  则呈相反趋势。然而，两个参数的亚组间差异均不显著。有趣的是，我们发现在所有三个亚群中  $\mu_0$  和  $G_0$  之间都有很高的相关性。这一发现表明，异常的运动神经元池兴奋性可能是通过整体突触输入和运动神经元的固有特性（如运动神经元池的导电性）的综合影响来调节的。尽管潜在的生理原因尚不清楚，但人们普遍认为过度活跃的拉伸反射与突触的变化有关，如突触前抑制的丧失和运动神经元内在特性的变化，这支持了我们的预测。

#### 4.5 局限性

对模型进行了几次简化。首先，它对运动过程中神经控制和肌肉骨骼系统的复杂相互作用进行了简化描述。因此，我们的目标是使用一个通用但有效的前向神经肌肉骨骼模型，该模型可以可靠地估计每个患者的被动肌腱和拉伸反射相关参数。有效性和敏感性分析表明，我们的模型可以以合理的计算效率充分模拟痉挛的被动伸腕测试。然而，我们意识到，当与电阻测量相结合时，神经生理学测量，如肌电图活动，可以提供更多关于痉挛的信息。此外，由于在测试过程中很少观察到伸肌的 EMG 信号，因此模型中不包括腕伸肌。其次，模型中没有考虑与拉伸无关的背景肌肉激活，这可能会导致高估 NC。先前的一项研究表明，在休息时，对照组和中风组的手腕肌肉都存在非零肌肉激活[43]。未来的工作应该考虑到背景肌肉激活。第三，由于未建模的装置传动系统的动力学，在快速运动中也注意到相当大的装置偏移。然而，我们发现，参与者之间的设备偏移量相似，这意味着在组比较的背景下，对模型参数估计的影响相当小。第四，操作仅在快速运动的一部分进行，在此期间收集验证的力数据。改进 NeuroFlexor 的机械设计在未来将是有益的。例如，在横向平面上延伸腕关节的修改可以消除手和手板的重力效应。此外， $B_p$  的估计也取决于手段惯性矩和角加速度估计的准确性，尽管粘性对总阻力扭矩的贡献很小。

## 5.结论

使用 forward 神经肌肉骨骼模型和优化，对慢性中风患者腕关节屈曲的神经和非神经相关特性进行了评估。该模型描述了在痉挛的被动伸展测试中腕关节的整体阻力行为。通过对数据的良好拟合、对参数波动的总体鲁棒性以及可用 EMG 测量和模型估计的一致性，证明了所提出的结合 NLS 最小化和基于启发式 GA 的搜索的优化方案的有效性。与对照组相比，抵抗扭矩的增加主要是由更高的被动刚度和反射诱导成分引起的。此外，在具有不同痉挛水平的参与者中，运动神经元池阈值和增益之间的相关性存在显著差异，这意味着异常的运动神经元池兴奋性可能由这两个参数的组合调节。我们得出的结论是，结合 NeuroFlexor 测量，所提出的神经肌肉骨骼模型和优化方案可以作为研究痉挛患者拉伸反射通路潜在参数变化的合适工具。这些参数具有物理意义，但不能直接测量。通过在治疗前后监测其值，可以为不同的干预策略提供有价值的见解。

## 道德许可

所有受试者均根据《赫尔辛基宣言》给予书面知情同意。这项研究得到了瑞典斯德哥尔摩卡罗琳斯卡研究所区域伦理委员会的批准。

## 利益冲突

我们声明潜在的利益冲突如下：本文中描述的 NF-方法已由 a.Fagergren 获得专利（WO\2008\121067）。作者 J.Gäverth 作为 Aggero MedTech AB 制造公司的股东，拥有本研究中描述的测量仪器的部分商业权利。

## 承诺

这项工作得到了斯德哥尔摩大脑研究所和 Promobilia 基金会的支持。我们感谢 Danderyd 医院康复医学部的 Gaia Valentina Pennati 分享控制数据。

## 补充材料

与本文相关的补充材料可以在在线版本中找到，网址为 doi:10.1016/j.medengphy.2017.06.023。

## 参考文献

- [1] Lance J . The control of muscle tone, reflexes, and movement: Robert Wartenberg Lecture. Neurology 1980;30:1303 .
- [2] Ashworth B . Preliminary trial of carisoprodol in multiple sclerosis. Practitioner 1964;192:540 – 2 .
- [3] Dietz V . Spastic movement disorder: what is the impact of research on clinical practice? J Neurol Neurosurg Psychiatry 2003;74:820 .
- [4] Gracies J . Pathophysiology of spastic paresis. I: Paresis and soft tissue changes. Muscle Nerve. 2005;31:535 .
- [5] Harlaar J , Becher J , Snijders C , Lankhorst G . Passive stiffness characteristics of ankle plantar flexors in hemiplegia. Clin Biomech 2000;15:261 .
- [6] Mirbagheri M , Barbeau H , Ladouceur M , Kearney R . Intrinsic and reflex stiffness in normal and spastic, spinal cord injured subjects. Exp Brain Res 2001;141:446 .
- [7] van der Helm F , Schouten A , de Vlugt E , Brouwn G . Identification of intrinsic

and reflexive components of human arm dynamics during postural control. *J Neurosci Methods* 2002;119:1 .

[8] de Vlugt E , de Groot JH , van der Heijden-Maessen HC , Wielheesen DH , van Wijlen-Hempel RMS , Arendzen JH , et al. Differentiation between non-neural and neural contributors to ankle joint stiffness in cerebral palsy. *J NeuroEng Rehabil* 2013;10:81 .

[9] Lorentzen J , Grey M , Crone C , Mazevet D , Biering-Sørensen F , Nielsen J . Distinguishing active from passive components of ankle plantar flexor stiffness in stroke, spinal cord injury and multiple sclerosis. *Clin Neurophys* 2010;121:1939 .

R. Wang et al. / *Medical Engineering and Physics* 47 (2017) 198 – 209 209

[10] Blanchette AK , Mullick AA , Moïn-Darbari K , Levin MF . Tonic stretch reflex threshold as a measure of ankle Plantar – Flexor spasticity after stroke. *Phys Ther* 2015 .

[11] Calota A , Feldman A , Levin M . Spasticity measurement based on tonic stretch reflex threshold in stroke using a portable device. *Clin Neurophys* 2008;119:2329 – 37 .

[12] Ju M , Chen J , Lee H , Lin T , Lin C , Huang Y . Time-course analysis of stretch reflexes in hemiparetic subjects using an on-line spasticity measurement system. *J Electromyogr Kinesiol* 2010;20:10:1 .

[13] Lindberg P , Gäverth J , Islam M , Fagergren A , Borg J , Forssberg H . Validation of a new biomechanical model to measure muscle tone in spastic muscles. *Neurorehabil Neural Repair* 2011;25:617 .

[14] Gäverth J , Sandgren M , Lindberg P , Forssberg H , Eliasson A . Test-retest and inter-rater reliability of a method to measure wrist and finger spasticity. *J Rehabil Med* 2013;45:630 .

[15] Gäverth J , Eliasson A , Kullander K , Borg J , Lindberg P , Forssberg H . Sensitivity of the NeuroFlexor method to measure change in spasticity after treatment with botulinum toxin A in wrist and finger muscles. *J Rehabil Med* 2014;46:629 .

[16] Katz R , Rymer W . Spastic hypertonia: mechanisms and measurement. *Arch Phys Med Rehabil* 1989;70:144 .

- [17] Powers R , Marder-Meyer J , Rymer W . Quantitative relations between hypertonia and stretch reflex threshold in spastic hemiparesis. *Annal Neurol* 1988;23:15 .
- [18] Sheean G . The pathophysiology of spasticity. *Eur J Neurol* 2002;9:3 – 9 .
- [19] Dietz V , Sinkjaer T . Spastic movement disorder: impaired reflex function and altered muscle mechanics. *Lancet Neurol* 2007;6:725 – 33 .
- [20] Hidler JM , Rymer WZ . A simulation study of reflex instability in spasticity: origins of clonus. *IEEE Trans Rehabil Eng* 1999;7:327 .
- [21] Koo TK , Mak AF . A neuromusculoskeletal model to simulate the constant angular velocity elbow extension test of spasticity. *Med Eng Phys* 2006;28:60 .
- [22] de Vlugt E , de Groot JH , Schenkeveld KE , Arendzen JH , van der Helm FC , Meskers CG . The relation between neuromechanical parameters and Ashworth score in stroke patients. *J NeuroEng Rehabil* 2010;7:35 .
- [23] van der Krogt H , Klomp A , de Groot JH , de Vlugt E , van der Helm FC , Meskers CG , et al. Comprehensive neuromechanical assessment in stroke patients: reliability and responsiveness of a protocol to measure neural and non-neural wrist properties. *J NeuroEng Rehabil* 2015;12 .
- [24] Kim C-S , Eom G-M , Hase K . Modeling and identification of mechanical and reflex properties related to spasticity in stroke patients using multiple pendulum tests. *J Biomech Sci Eng* 2011;6:135 – 47 .
- [25] Winters J , Stark L . Analysis of fundamental human movement patterns through the use of in-depth antagonistic muscle models. *IEEE Trans Biomed Eng* 1985;32:826 .
- [26] Robertson G , Caldwell G , Hamill J , Kamen G , Whittlesey S . Research methods in biomechanics. 2nd ed. Human Kinetics; 2013 .
- [27] Prochazka A , Gorassini M . Models of ensemble firing of muscle spindle afferents recorded during normal locomotion in cats. *J Physiol* 1998;507:277 .
- [28] Wilson L , Gandevia S , Inglis J , Gracies J , Burke D . Muscle spindle activity in the affected upper limb after a unilateral stroke. *Brain J Neurol* 1999;122:2079 .
- [29] Fuglevand A , Winter D , Patla A . Models of recruitment and rate coding organization in motor-unit pools. *J Neurophys* 1993;70:2470 .

- [30] Thelen DG . Adjustment of muscle mechanics model parameters to simulate dynamic contractions in older adults. J Biomech Eng 2003;125:70 – 7 .
- [31] Golberg DE . Genetic algorithms in search, optimization, and machine learning 1989 1989 .
- [32] Macefield V . Discharge rates and discharge variability of muscle spindle afferents in human chronic spinal cord injury. Clin Neurophys 2013;124:1 14 .
- [33] Wang R , Gutierrez-Farewik E . Compensatory strategies in response to excessive muscle co-contraction at the ankle joint during walking. Gait Posture 2014;39:926 – 32 .
- [34] De Serres S , Milner T . Wrist muscle activation patterns and stiffness associated with stable and unstable mechanical loads. Exper Brain Res 1991;86:451 .
- [35] Gielen C , Houk J . Nonlinear viscosity of human wrist. J Neurophys 1984;52:553 .
- [36] Fukashiro S , Komi P , Järvinen M , Miyashita M . Comparison between the directly measured Achilles tendon force and the tendon force calculated from the ankle joint moment during vertical jumps. Clin Biomech 1993;8:25 – 30 .
- [37] Heckman C , Binder MD . Computer simulation of the steady-state input – output function of the cat medial gastrocnemius motoneuron pool. J Neurophysiol 1991;65:952 – 67 .
- [38] Niu CM , Nandyala SK , Sanger TD . Emulated muscle spindle and spiking afferents validates VLSI neuromorphic hardware as a testbed for sensorimotor function and disease. Front Comput Neurosci 2014;8 .
- [39] Winters J , Bagley A . Biomechanical modeling of muscle-joint systems. IEEE Eng Med Biol Mag 1987;6:17 .
- [40] Hamill J., Knutzen K.M. Biomechanical basis of human movement Lippincott Williams & Wilkins; 2006.
- [41] Bagni M , Cecchi G , Colomo F , Garzella P . Absence of mechanical evidence for attached weakly binding cross-bridges in frog relaxed muscle fibres. J Physiol 1995;482:391 .
- [42] Halar E , Stolov W , Venkatesh B , Brozovich F , Harley J . Gastrocnemius muscle



belly and tendon length in stroke patients and able-bodied persons. Arch Phys Med Rehabil 1978;59:476 .

[43] Helgadottir A . Identification of muscle activation at rest Master thesis. Delft University of Technology; 2013 .

[44] Lieber R , Runesson E , Einarsson F , Fridén J . Inferior mechanical properties of spastic muscle bundles due to hypertrophic but compromised extracellular matrix material. Muscle Nerve 2003;28:464 .

## 参考文献原文



# Neural and non-neural related properties in the spastic wrist flexors: An optimization study



R. Wang<sup>a,b,d,\*</sup>, P. Herman<sup>c</sup>, Ö. Ekeberg<sup>c</sup>, J. Gäverth<sup>d</sup>, A. Fagergren<sup>e</sup>, H. Forssberg<sup>d</sup>

<sup>a</sup> Department of Mechanics, Royal Institute of Technology, Stockholm, Sweden

<sup>b</sup> KTH Biomex Center, Royal Institute of Technology, Stockholm, Sweden

<sup>c</sup> Dept. of Computational Science and Technology, Royal Institute of Technology, Stockholm, Sweden

<sup>d</sup> Department of Women's and Children's Health, Karolinska Institutet, Stockholm, Sweden

<sup>e</sup> AggeroMedTech AB, Stockholm, Sweden

## ARTICLE INFO

### Article history:

Received 2 September 2016

Revised 14 June 2017

Accepted 14 June 2017

### Keywords:

Stroke

Stretch reflex

Constant angular velocity

Optimization

NeuroFlexor

## ABSTRACT

Quantifying neural and non-neural contributions to increased joint resistance in spasticity is essential for a better understanding of its pathophysiological mechanisms and evaluating different intervention strategies. However, direct measurement of spasticity-related manifestations, e.g., motoneuron and biophysical properties in humans, is extremely challenging. In this vein, we developed a forward neuromusculoskeletal model that accounts for dynamics of muscle spindles, motoneuron pools, muscle activation and musculotendon of wrist flexors and relies on the joint angle and resistant torque as the only input measurement variables. By modeling the stretch reflex pathway, neural and non-neural related properties of the spastic wrist flexors were estimated during the wrist extension test. Joint angle and resistant torque were collected from 17 persons with chronic stroke and healthy controls using NeuroFlexor, a motorized force measurement device during the passive wrist extension test. The model was optimized by tuning the passive and stretch reflex-related parameters to fit the measured torque in each participant. We found that persons with moderate and severe spasticity had significantly higher stiffness than controls. Among subgroups of stroke survivors, the increased neural component was mainly due to a lower muscle spindle rate at 50% of the motoneuron recruitment. The motoneuron pool threshold was highly correlated to the motoneuron pool gain in all subgroups. The model can describe the overall resistant behavior of the wrist joint during the test. Compared to controls, increased resistance was predominantly due to higher elasticity and neural components. We concluded that in combination with the NeuroFlexor measurement, the proposed neuromusculoskeletal model and optimization scheme served as suitable tools for investigating potential parameter changes along the stretch-reflex pathway in persons with spasticity.

© 2017 IPEM. Published by Elsevier Ltd. All rights reserved.

## 1. Background

Spasticity is a motor disorder that is commonly seen in many neurological disorders. It is clinically defined as a velocity-dependent increase in tonic stretch reflex with exaggerated tendon jerks, resulting from hyper-excitability of the stretch reflex [1]. In current practice, spasticity is commonly measured subjectively by rotating a joint and estimating the resistance according to an ordinal scale, such as the Modified Ashworth Score (MAS) [2]. Previous reports indicate that the intrinsic mechanical properties

of the muscle and tendon may also be altered secondary to spasticity, and may thereby also contribute to the increased joint resistance [3,4]. Thus, the limited reliability and reproducibility of the MAS and the impossibility of discriminating between the underlying neural contributions (the stretch reflex) and the non-neural contributions have motivated the development of alternative methods to quantify resistant joint torque objectively [5–7]. Several laboratories have developed custom-built apparatuses to examine joint stiffness in terms of underlying neural and mechanical properties, mostly at the ankle joint [8–10] and elbow joint [11,12]. Recently, Lindberg et al. developed a mechanical device that functions as an instrumented version of the MAS test to quantify spasticity of the wrist flexors at rest. This test is also convenient for daily clinical practice [13]. The NeuroFlexor instrument (Aggero MedTech AB, Solna Sweden) passively extends the wrist at two different constant velocities. A force transducer measures the resistance throughout the movements. The NeuroFlexor real-time anal-

\* Corresponding author at: Department of Mechanics, Royal Institute of Technology, Stockholm, Sweden.

E-mail addresses: [ruoli@kth.se](mailto:ruoli@kth.se) (R. Wang), [paherman@kth.se](mailto:paherman@kth.se) (P. Herman), [ekeberg@kth.se](mailto:ekeberg@kth.se) (Ö. Ekeberg), [johan.gaverth@ki.se](mailto:johan.gaverth@ki.se) (J. Gäverth), [anders.fagergren@aggeromedtech.com](mailto:anders.fagergren@aggeromedtech.com) (A. Fagergren), [Hans.Forssberg@ki.se](mailto:Hans.Forssberg@ki.se) (H. Forssberg).

ysis method (NF-method) [13], can separate the contributions to the measured resistant torque into the passive elastic torque, passive viscous torque, and reflex torque (see *Supplementary file A*). The NF-method was validated in chronic stroke patients and demonstrated a strong correlation between the neural component and the flexor carpi radialis (FCR) activity in electromyography (EMG), both across subjects and in each subject during a nerve block test [13]. Recent investigations have also demonstrated that the NF-method is reliable [14] and sensitive enough to detect changes in spasticity after treatment with botulinum toxin in stroke patients [15].

Several theories have been proposed to explain the cause of spasticity, including a decreased threshold or increased gain of the stretch reflex, hyper-excitability of the  $\alpha$ -motor neurons, and hyper-sensitivity of the muscle spindles [16–18]. Although decades of neurophysiological research have enriched our understanding of spasticity, the reported data have been contradictory at times [19]. Overall, the pathophysiological mechanisms of spasticity are still a matter of debate, and direct measurement of the motoneuron and biophysical properties of humans is not possible [20]. As such, researchers have attempted to develop biomechanical and theoretical models to facilitate the investigation of the mechanisms of spasticity. The models vary in complexity and rely on different experimental protocols. Koo and Mak [21] developed a neuromusculoskeletal model to simulate the stretch reflex response induced during an extension of elbow joint at constant angular velocity. They analyzed the effects of model parameters such as the motoneuron pool thresholds and gain on the biomechanical behavior of the elbow joint. The outcome was based on one hemiparetic subject with only mild spasticity. De Vlugt et al. [22] quantified the viscosity, stiffness, and reflex torques of the ankle joint using a nonlinear model combined with motorized assessment and EMG. They found significant differences in elasticity and viscosity between stroke patients and controls. They also developed a comprehensive assessment protocol that includes passive, active, and reflexive tests to measure neural and non-neural contributors to movement disorders at the wrist after stroke [23]. However, the motoneuron pool or muscle spindle behavior could not be investigated. Kim et al. [24] proposed a model that characterizes the stretch reflex system as a velocity feedback loop, and could identify spastic and intrinsic properties of the knee joint. The study was based on the pendulum test, which is usually only applicable for knee muscle spasticity.

Our aims were to build a forward neuromusculoskeletal model that incorporates the stretch reflex loop of the wrist flexors and to demonstrate the feasibility of the proposed modeling and optimization framework for investigating the potential pathophysiological mechanisms of spasticity. The model accounts for the properties of the musculotendon, muscle spindles, and motoneuron pool of the wrist flexors. The optimization requires only the measured joint angle and resistant torque as input variables. The proposed computational approach could be extensively validated on a sizable sample of participants with stroke and healthy controls. Thus, the main objectives of our modeling efforts were (1) to examine the model-identified components related to the stretch reflex and muscle mechanics and the correlations with their counterparts obtained from the NF-method, and (2) to identify the potential spasticity-related manifestations in terms of changes in the motoneuron pool and muscle spindle behavior in persons with stroke with spasticity of varying severity.

## 2. Method

### 2.1. Subjects

A sample of 17 persons with chronic stroke (ST) (mean  $\pm$  SD, age:  $50 \pm 11$  yr, body weight:  $79 \pm 10$  kg) was selected from

previous studies, in which NeuroFlexor data had been collected [14,15] (Table 1). A total of 17 healthy persons (age:  $48 \pm 10$  yr, weight:  $79 \pm 12$  kg) without any history of neurological disorder were selected as controls. Due to the heterogeneity in the ST, it was further divided into three subgroups according to the neural component (NC) identified using the NF-method, i.e., the participants with low spasticity (STL,  $NC \leq 10$  N); with moderate spasticity (STM,  $10 \text{ N} < NC < 30$  N); and with severe spasticity (STH,  $NC \geq 30$  N). Additional five participants with stroke having simultaneous NeuroFlexor and EMG recordings of the FCR were selected as a validation group.

### 2.2. Experimental setup and protocol

The resistance torque was measured using the NeuroFlexor, a portable computer-controlled servo-motor system including a high resolution step motor and a motor controller that produced constant movements at a slow ( $5^\circ \text{ s}^{-1}$ ) and a fast ( $236^\circ \text{ s}^{-1}$ ) velocity (see details in [13] and *Supplementary file B*). The range of wrist movement was set from  $20^\circ$  flexion and to  $30^\circ$  extension for all participants. For the additional 5 participants in the validation group, surface EMG was recorded from the FCR (MYO 15, Liberty Technology, Hopkinton, Massachusetts). To avoid noise amplification, raw torque and angle data were low pass filtered with a cut-off frequency of 10 Hz (second-order Butterworth filter). All participants gave written informed consent according to the Declaration of Helsinki. The study was approved by the Regional Ethics Committee, Karolinska Institutet, Stockholm, Sweden.

### 2.3. Neuromusculoskeletal model

Our neuromusculoskeletal model includes components that describe the dynamics of musculotendon, muscle spindle, motoneuron pool, and muscle activation of the wrist flexors (Fig. 1).

#### 2.3.1. Musculotendon modeling

The musculotendon model consisted of one lumped muscle actuator that represents synergistic wrist flexors and one passive unit [25]. Wrist extensors were not included in the model due to their negligible activation during the passive wrist extension movement.

*Equation of motion:* The modeled wrist resistant torque was determined according to dynamic equilibrium during the passive wrist extension movement:

$$T_m = (J_h + J_{hp})\ddot{\theta} + T_{MA} + T_{PP} + T_{Ch} + T_{Ghp} \quad (1)$$

with  $T_m$  the modeled resistant moment,  $J_h$  and  $J_{hp}$  the moments of inertia of the hand segment and hand-plate,  $\ddot{\theta}$  the angular acceleration,  $T_{MA}$  the torque generated by the lumped muscle actuator,  $T_{PP}$  the torque generated by the passive unit, and  $T_{Ch}$  and  $T_{Ghp}$  the torques due to the gravity of the hand segment and hand-plate, respectively,

$$J_h = m_h(K_{cg}l_h)^2 + m_h(K_{proximal}l_h)^2 \quad (2)$$

The moment of inertial of the hand segment was estimated based on the mass ( $m_h$ ) and length ( $l_h$ ) of the hand, and the length of radius of gyration as a proportion of the hand length about the center of gravity ( $K_{cg}$ ) and the proximal joint ( $K_{proximal}$ ) [26]. The moment of inertial of the hand-plate was estimated using the initial resistance torque offset.

*Passive unit:* The passive unit in the model was considered as the passive viscoelastic elements of the muscle and connective tissues of the joint [25]:

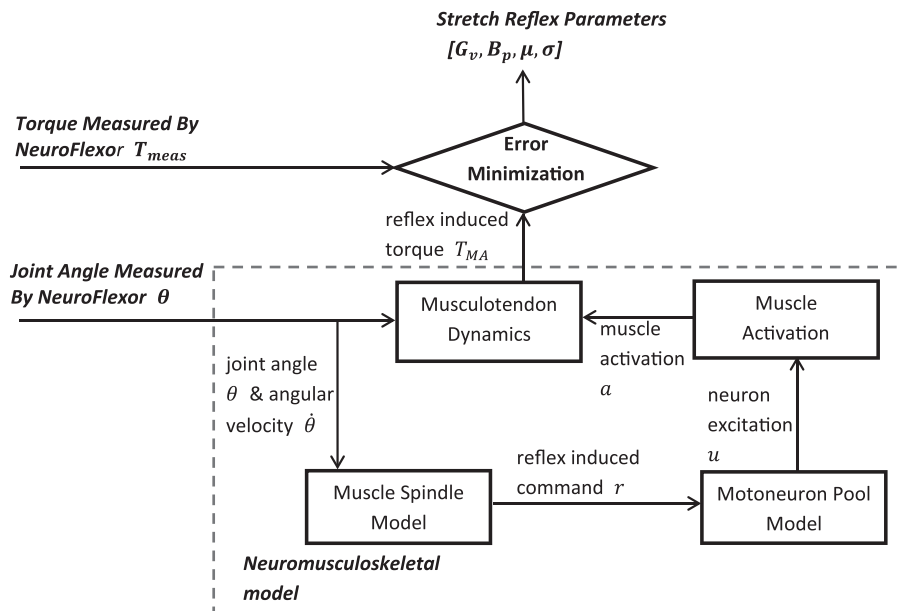
$$T_{PP} = K_p(\theta - \theta_0) + B_p\dot{\theta} + k_1 e^{k_2(\theta - \theta_0) - 1} \quad (3)$$

with  $K_p$  the stiffness coefficient,  $B_p$  the viscosity coefficient,  $k_1$  and  $k_2$  the non-linear exponential coefficients, and  $\theta_0$  the resting joint

**Table 1**

Clinical description of participants (ST: persons with stroke, C: controls, V: validation subjects).

Participants	Gender	Age (Years)	Weight (Kg)	Lesion Type	Post Stroke Time (Months)	Modified Ashworth Score
ST1	M	66	87	Ischemic	86	1
ST2	M	57	82	Ischemic	120	3
ST3	F	30	83	Trauma	111	3
ST4	F	62	60	Ischemic	114	4
ST5	M	43	77	Ischemic	37	4
ST6	M	56	96	Haemorrhagic	123	3
ST7	F	55	74	Haemorrhagic	55	4
ST8	M	45	75	Ischemic	10	0
ST9	M	47	100	Ischemic	28	3
ST10	M	44	80	Haemorrhagic	36	3
ST11	M	63	71	Ischemic	10	2
ST12	M	59	69	Ischemic	50	2
ST13	M	51	75	Haemorrhagic	12	3
ST14	M	46	84	Haemorrhagic	44	1
ST15	M	47	82	Haemorrhagic	16	4
ST16	M	61	78	Haemorrhagic	7	3
ST17	M	22	75	Haemorrhagic	20	4
C1	M	36	75	–	–	–
C2	F	38	65	–	–	–
C3	F	60	60	–	–	–
C4	F	36	75	–	–	–
C5	F	32	70	–	–	–
C6	F	32	60	–	–	–
C7	M	47	78	–	–	–
C8	M	47	85	–	–	–
C9	M	47	108	–	–	–
C10	M	49	92	–	–	–
C11	M	50	90	–	–	–
C12	M	55	82	–	–	–
C13	M	55	89	–	–	–
C14	M	55	70	–	–	–
C15	M	58	82	–	–	–
C16	M	58	80	–	–	–
C17	M	59	90	–	–	–
V1	M	40	88	Haemorrhagic	55	1+
V2	M	61	87	Haemorrhagic	75	0
V3	F	66	79	Haemorrhagic	43	3
V4	F	72	80	Ischemic	86	4
V5	F	63	69	Haemorrhagic	90	2

**Fig. 1.** The diagram of the neuromusculoskeletal modeling to quantify passive stretch reflex parameters using optimization. The neuromusculoskeletal model includes components that describe the dynamics of musculotendon, muscle spindle, motoneuron pool, and muscle activation of the wrist flexors.

angle at the muscle-tendon slack length, such that,  $T_{pp}$  is equal to zero.

The elasticity component (EC) was an angle-dependent torque component of  $T_{pp}$ , and the viscosity component (VC) was an angular velocity-dependent torque component,

$$EC = K_p(\theta - \theta_0) + k_1 e^{k_2(\theta - \theta_0) - 1} \quad (4)$$

and

$$VC = B_p \dot{\theta} \quad (5)$$

**Lumped muscle actuator:** The lumped muscle actuator was modeled as a contractile element in series with a series elastic element. The joint moment-angle and moment-angular velocity relationships were implemented in the actuator model [25].

$$T_{MA} = a f_v(\dot{\theta}) f_l(\theta) \quad (6)$$

with  $a$  the muscle activation (see *Muscle activation dynamics*),  $f_v$  the moment-angular velocity relationship, and  $f_l$  the moment-angle relationship. In passive wrist extension, muscle activation  $a$  was considered entirely induced by the stretch reflex of the wrist flexors. Therefore, the neural component (NC) was equivalent to  $T_{MA}$ .

### 2.3.2. Muscle spindle modeling

The modified hybrid  $v^{0.6}$  model [27] was implemented to describe the firing characteristics of the muscle spindle in lengthening as a function of joint angle and angular velocity:

$$r(t) = G_v(\dot{\theta}(t - \tau_{SRD}))^{0.6} + G_l(\theta(t - \tau_{SRD}) - \theta_0) + r_0 \quad (7)$$

with  $r$  the Ia afferent (the primary afferent) firing rate,  $\theta_0$  the rest joint angle,  $\tau_{SRD}$  the stretch reflex delay,  $G_v$  and  $G_l$  the dynamic and static gains of the spindle model, respectively, and  $r_0$  the background discharge rate of the Ia afferent neuron.  $\tau_{SRD}$  and  $r_0$  were set to 30 ms and  $6.45 \text{ imps}^{-1}$  [28].

### 2.3.3. Motoneuron pool modeling

The input-output relationship for the  $\alpha$ -motoneuron pool was represented by a Gaussian cumulative distribution function [29]. As previously reported [21], we also assume that all synaptic inputs to the  $\alpha$ -motoneuron pool except those from muscle spindle can be considered as constant in the passive movement and that the synaptic current elicited by the spindle is linearly scaled to the spindle firing rate. Therefore, the motoneuron pool transformation, representing the motoneuron neural excitation as a function of the muscle spindle firing rate, was modeled as a sigmoid function which ranges from 0 to 1,

$$u(t) = \frac{1}{1 + e^{\frac{\mu - r(t)}{\sigma}}} \quad (8)$$

with  $u$  the neural excitation of the motoneuron pool,  $\mu$  the muscle spindle firing rate at 50% motoneuron recruitment, and  $\sigma$  the standard deviation of cumulative distribution function.

For better interpretation and more physiological meaningful, the threshold and gain of the motoneuron pool of wrist flexors were further calculated based on the definition from a previous study [21]. A threshold  $\mu_0$  corresponds to the spindle-firing rate that results in neural excitation of 0.005, and gain  $G_0$  is defined:

$$G_0 = \frac{0.6}{r_{0.8} - r_{0.2}} \quad (9)$$

with  $r_{0.8}$  and  $r_{0.2}$  the muscle spindle firing rate at 80% and 20% of full motoneuron recruitment.

### 2.3.4. Muscle activation dynamics

Activation dynamics was described as the process of converting neural excitation  $u(t)$  to muscle activation  $a(t)$  as a first order differential equation [30]:

$$\dot{a}(t) = \frac{u(t) - a(t)}{\tau(a(t), u(t))} \quad (10)$$

$$\tau(a(t), u(t)) = \begin{cases} \tau_{act} (1.5a(t) + 0.5) & u(t) > a(t) \\ \tau_{dact} / (1.5a(t) + 0.5) & u(t) \leq a(t) \end{cases} \quad (11)$$

with  $\tau$  the time constant that varies with activation level and the dynamics of muscle activation level (increasing or decreasing), and  $\tau_{act}$  and  $\tau_{dact}$  the activation and deactivation time constants.

## 2.4. Optimization

There were four passive joint parameters [ $K_p$ ,  $B_p$ ,  $k_1$ ,  $k_2$ ] and four stretch reflex related parameters [ $G_v$ ,  $G_l$ ,  $\mu$ ,  $\sigma$ ] needed to be tuned for each participant in the model.

### 2.4.1. Passive parameters

It was assumed that muscle resistant torque induced by the stretch reflex was negligible during the slow movement; hence the resistant torque was entirely caused by the passive unit. Nonlinear least-squares (NLS) optimization was used to approximate the passive parameters based on the experimental measurements of the resistant torque in the slow movement. The initial values of these parameters were obtained from literature [25]:  $K_p = 1 \text{ Nm/rad}$ ,  $B_p = 0.1 \text{ Nms/rad}$ ,  $k_1 = 0.37 \text{ Nm}$ ,  $k_2 = 3.44 \text{ rad}^{-1}$ . The initial 0.5 s and the last 2 s of the slow movement were eliminated from the analysis to avoid the acceleration and deceleration phase of the measurement. The viscosity coefficient  $B_p$  was further corrected by minimizing the differences between the modeled and measured resistant torque assuming the negligible stretch-reflex induced torque at the first peak of the fast movement (PI, Fig. 4).

### 2.4.2. Stretch reflex related parameters

A genetic algorithm (GA) [31] was used to identify the optimal stretch reflex-related parameters by minimizing the root-mean-square error (RMSE) between the measured and modeled resistant torque in part of the fast movement. GA is an optimization method based on the concept of natural selection imitating biological evolution. The GA in this study was configured with double-precision floating-point representation, additive mutation drawn from Gaussian distribution, single-point crossover and stochastic uniform selection [31]. A pilot sensitivity analysis was performed in 10 randomly selected participants from the ST group to determine the basic parameters for GA: population size (50), crossover (0.8) and mutation fraction (0.1) as well as the maximum number of generations (100) for convergence. In order to obtain reliable optimal stretch reflex related parameters, GA was repeated 10 times starting from a different initial population for each individual trial for each participant. The final selected parameters corresponded to the best solution found, i.e., the solution with the minimal RMSE.

In calculation of the fitness function (the aforementioned RMSE), the device offset was included in the predicted resistant torque, defined as the differences between modeled and measured resistant torque without the hand during the fast movement. Since the static and dynamic gains of the muscle spindle in the pathological group were shown to be similar to those from healthy controls [32], constraints were imposed on  $G_v$  and  $G_l$  to vary  $\pm 10\%$  from the reported values (4.3 and 2.0, respectively).

## 2.5. Data analysis and statistics

A set of representative trials from each participant's NeuroFlexor measurements (one slow movement, one fast movement, one slow movement without the hand and one fast movement without the hand) was selected to calculate the EC, VC and NC using both NF-method and optimization. The same trials were also used for computing passive and stretch-reflex related parameters using the neuromusculoskeletal model and optimization. The raw EMG data was sampled at 1000 Hz, rectified and linear enveloped (2nd order bi-directional Butterworth filter with cut-off frequency at 6 Hz) [33].

The validity of the model was determined for each trial by the Variance Accounted For (VAF) and the coefficient of determination ( $R^2$ ), which describe the 'goodness of fit' of the simulated and measured resistant torque [22]:

$$VAF = \left(1 - \frac{\sum \epsilon(t)^2}{\sum T_{meas}(t)^2}\right) \cdot 100\% \quad (11)$$

$$R^2 = 1 - \frac{\sum \epsilon(t)^2}{\sum (T_{meas}(t) - \bar{T}_{meas})^2} \quad (12)$$

with  $\epsilon(t)$  the error, i.e. the difference between the measured resistant torque,  $T_{meas}(t)$  and the modeled resistant torque,  $T_m(t)$ , over  $t = 1, \dots, N$  samples, and  $\bar{T}_{meas}$  the mean of the measured resistant torque.

To verify the generalization aspect of the model fitting, the VAF was also determined in three extra sets of measurement trials from each participant using the passive and stretch-reflex related parameters obtained from the optimization. We also examined the sensitivity of the model with respect to the passive and stretch reflex-related parameters by calculating the sensitivity index (SI), as discussed in detail in *Supplementary file C*.

Descriptive statistics were expressed as median and range. Non-parametric statistical tests were used throughout the study. Spearman's rank order correlation test was used to investigate the correlation between components identified by the NF-method and optimization, respectively. To test the between-group differences, Mann-Whitney U test was used. To test the differences in passive and stretch reflexed related parameters between HC group and subgroups of participants with stroke, Kruskal-Wallis H test was used. A post-hoc pairwise comparison with Bonferroni adjustment was applied if the omnibus test was significant.

## 3. Results

### 3.1. Passive parameters

During the slow movement, the total resistant torque increased linearly when the wrist was passively extended from the initial position and showed a slightly exponential increase when the joint was extended towards the maximal measurement angle. As an example, Fig. 2(B) shows the modeled and measured total resistant torque of one participant with stroke and one healthy control during the slow movement. It illustrated a good fit of the model and consistent findings were observed in all participants (Table 2). The VAF value of the extra sets of trials was similar as the trials used for optimization (ST:  $99.2\% \pm 1.8\%$ , Control:  $99.4\% \pm 1.5\%$ ), which validated the generalization properties of the model fitted to individual participant.

Compared to controls, participants with stroke had significantly higher stiffness coefficient  $K_p$  ( $p < 0.01$ ) and non-linear coefficients  $k_1$  ( $p = 0.031$ ). Further subgroup comparisons showed that  $K_p$  and  $k_1$  of the STL group were similar to those in the control group, but they were significantly higher in STM and STH groups than in control group (Fig. 3 and Table 3).

**Table 2**

The Variance Accounted For (VAF) and the coefficient of determinations ( $R^2$ ) between modeled and measured resistant torque during the slow and fast movement.

Mean (S.D)	Slow movement		Fast movement	
	VAF	$R^2$	VAF	$R^2$
Control	98.12% (2.11%)	0.99 (0.002)	N/A	
ST	98.62% (2.30%)	0.99 (0.003)	98.23% <sup>a</sup> (1.39%)	0.89 (0.04)

<sup>a</sup> The average VAF value was calculated when two outliers in the STL group were excluded.

### 3.2. Stretch reflex-related parameters

Due to measurement error during the period 0.05–0.09 s of the recording and the latency of the reflex, the optimization was only performed for a selected part of the fast movement (from the second peak, PII, to the third peak, PIII, of the measured total resistant torque, Fig. 4(B)), during which the angular velocity remained stable (Fig. 4(A)). The stretch reflex-related parameters were only identified in the ST group. As an example, Fig. 4(B) shows the modeled and measured resistant torque of one participant with stroke during the fast movement. It also illustrated a good fit of the model to the data. Consistent findings were observed in all participants except two outliers in the STL group (Table 2). The VAF value of the extra sets of trials was similar as the trials used for optimization ( $95.4\% \pm 3.5\%$ ). Moreover, as showed in the example of one patient, the onset timing of FCR agrees with modeled estimated muscle activity timing in the validation group (Fig. 5).

Two motoneuron pool parameters ( $\mu$  and  $\sigma$ ) showed having a decreasing tendency with increasing level of spasticity in the groups of stroke survivors (Table 3). Significant differences in  $\mu$  between mildly and severely affected groups ( $p = 0.01$ ) were observed, but not in  $\sigma$ .

The participants with more severer spasticity had somewhat lower motoneuron pool threshold  $\mu_0$  and higher gain  $G_0$ , but differences were not significant. Significant and very high correlations between  $\mu_0$  and  $G_0$  were determined in all three subgroups (STL:  $p < 0.01$ ,  $r = 0.99$ , STM:  $p < 0.01$ ,  $r = 0.90$ , STH:  $p < 0.01$ ,  $r = 0.96$ , Figs. 6 and 7).

### 3.3. Correlation of individual components from model estimation and the NF-method

The EC, VC and NC were identified in the groups of stroke survivors at the third peak of the resistant torque in the fast movement (PIII, Fig. 4(B)), the same as the NF-method. The individual components calculated from the current model estimation correlated well with those based on the NF-method (Fig. 8). A significant and very high correlation was determined in NC ( $p < 0.01$ ,  $r = 0.94$ ), high correlation in EC ( $p < 0.01$ ,  $r = 0.84$ ), and moderate correlation in VC ( $p < 0.01$ ,  $r = 0.70$ ).

## 4. Discussion

We built a neuromusculoskeletal model to simulate a passive wrist extension test of spasticity. By modeling the musculotendon, muscle spindle, and motoneuron pool parameters explicitly, the neural and non-neural related properties at the wrist joint were estimated in persons with chronic stroke using optimization techniques. Compared to the controls, the stroke survivors exhibited higher passive stiffness. The motoneuron pool parameters tended to decrease with increased spasticity. In addition, the motoneuron pool threshold and gain were highly correlated in all three subgroups. To the best of our knowledge, this is the first study that



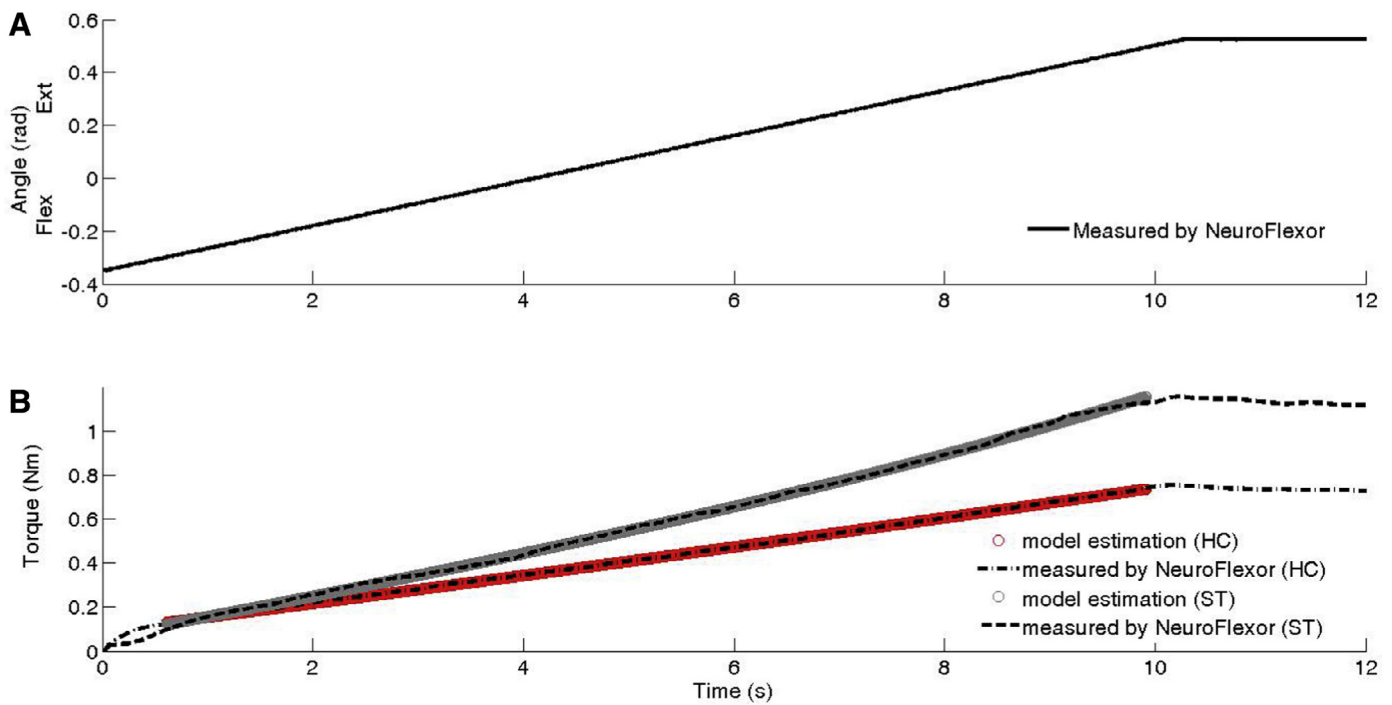


**Fig. 2.** (A) In the slow movement, the wrist joint was passively extended from  $20^\circ$  ( $0.35$  rad) to  $30^\circ$  ( $0.52$  rad) of extension at  $5^\circ/\text{s}$  using a NeuroFlexor. (B) A nonlinear-least squares optimization was used to predict passive parameters by fitting to the torque measured in the slow movement. The black dashed and dotted-dashed lines represent the measured resistant torque of a representative healthy subject and a stroke patient, respectively. The lines with gray and red circles represent the modeled resistant torque for the same subject. (For interpretation of the references to colour in this figure legend, the reader is referred to the web version of this article.)

has attempted to investigate the potential underlying mechanics of wrist muscle spasticity by combining motorized measurements and neuromusculoskeletal modeling, with the joint angle and resistant torque as the only input measurement variables.

#### 4.1. Validity of the method

The neuromusculoskeletal model was first verified using VAF. The VAF values were above 90% for all participants (except two outliers in the STL group) for both slow and fast movements. We also found a very high correlation between the modeled and measured resistant torque (Table 2). The high values of VAF and the coefficient of determination indicated that the overall model was robustly optimized to make reliable predictions of the total resistant torque during the current testing condition. The passive wrist stiffness and viscosity for healthy people were reported in the range of  $0.32$ – $0.41$  Nm/rad and  $0.02$ – $0.04$  Nms/rad [34,35]. No comparable data were found for stroke survivors in the literature. Due to the different testing conditions and modeling methods, direct comparison with other results was not suitable. Nevertheless, the modeled stiffness and viscosity in the current study were in the range of the reported values.

Unlike most other studies using EMG recordings to directly quantify neural contributions to joint resistance [8,9,22,36], the stretch reflex properties were estimated by modeling the muscle spindle and motoneuron pool explicitly. For validation, we included five additional participants with the EMG recording of FCR. The timing of the model-estimated muscle activity agreed with the recorded EMG responses (Fig. 5). The benefit of the proposed approach is that EMG recording is not necessary, which makes our method more practical and useful in daily clinical practice. Moreover, it still allows for investigation of the underlying spasticity mechanism since the overall input–output relationship of the motoneuron pool can be quantified.

It is also possible to gain insight into the reliability of the parameter estimation via the interdependence of the parameters by comparing the auto-covariance to the cross-covariance components for given parameters. The results shed light on the interactions between the parameters that are instrumental to the explanation of the variance of the model output. Low interdependence means parameter estimation is reliable [22]. We found that the auto-covariance is higher than the corresponding cross-covariance factors for all eight parameters, which indicates that the parameter estimation is reliable. Moreover, the model tended to be more sensitive to  $K_p$  and  $\mu$  than to the other passive parameters and those related to stretch reflex related, though the overall estimates suggested a moderate effect size (Table S1, Supplement file C).

#### 4.2. Model consideration

Regardless of the complexity of the neural circuit involved in the passive stretch reflex loop, the modeling of the reflex loop was simplified and consisted of muscle spindle and motoneuron pool models. The input–output properties of the mammalian motoneuron pool are still unknown, but, computer simulations of the motoneuron pool derived from steady-state conditions have shown good qualitative agreement with experimental data in animals [29,37]. Previous research has demonstrated the utility of the simplified structure of the spindle model to produce physiologically realistic behavior in human muscle spindles as well [38]. The static and dynamic gain of the hybrid  $V^{0.6}$  model reflected the level of  $\gamma$ -motoneuron activation. Recent research has shown that the firing rate of muscle spindles in persons with stroke was similar to those of the controls [3]. Therefore, we assumed that the sensitivity of the muscle spindle has a minor influence on the stretch reflex, and thus on the level of spasticity. The hyperactive stretch reflex was mainly due to the abnormal input–output relationship of the motoneuron pool. The characteristic parameters of the motoneuron pool (threshold and gain) should be interpreted as the

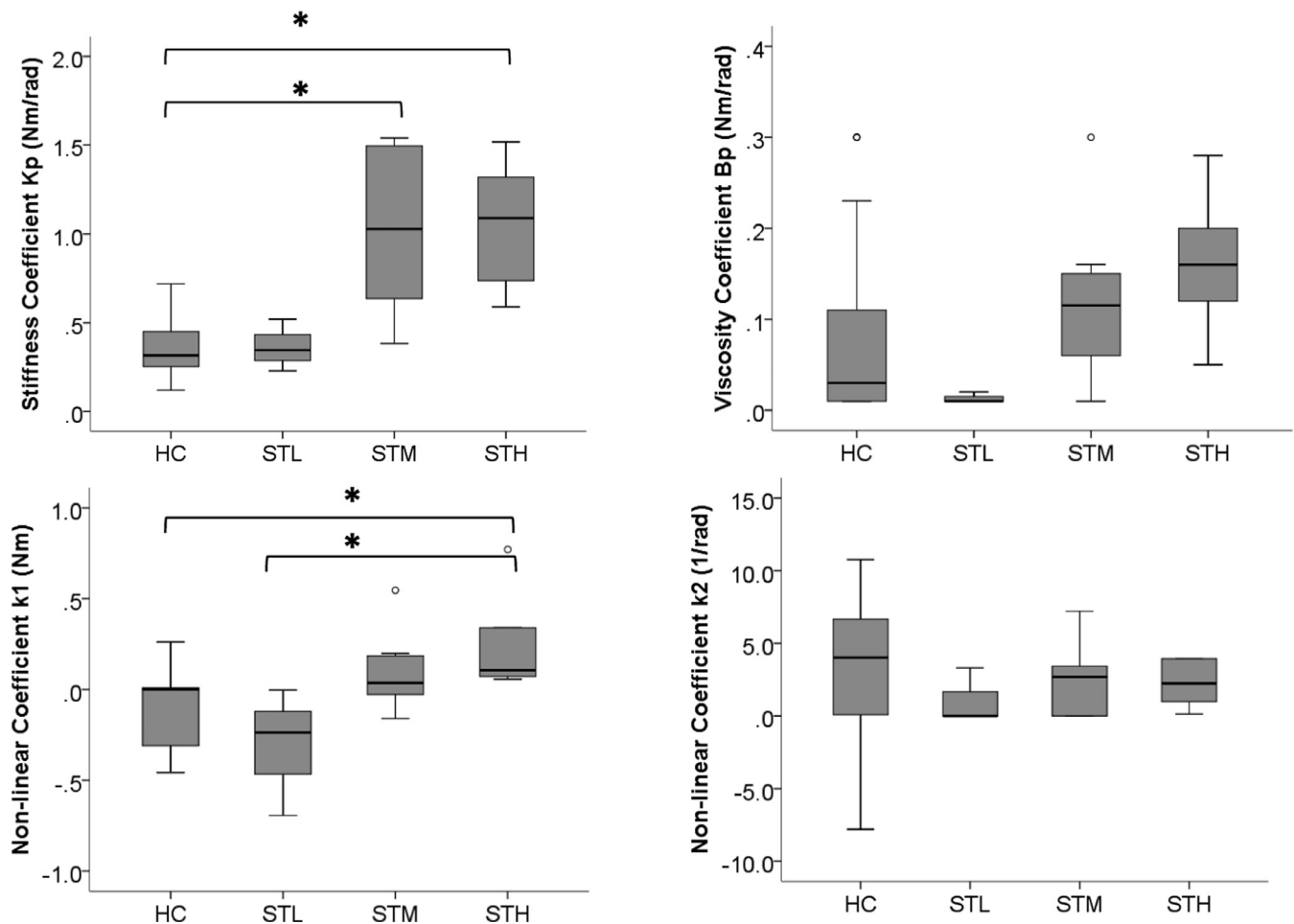


**Fig. 3.** Estimated stiffness coefficient  $K_p$ , viscosity coefficient  $B_p$ , and two non-linear coefficients  $k_1$  and  $k_2$  in the control group (HC), and in the stroke groups with mild (STL), moderate (STM) and severe (STH) spasticity as a box plot. The asterisk denotes significant differences between groups. The open circle denotes the outlier.

overall effects of all excitatory and inhibitory inputs that synapse directly or indirectly onto the motoneuron pool such as presynaptic inhibition, reciprocal inhibition and  $\alpha$ -motoneuron excitability, similar to a previous modeling approach [21].

A lumped parametric musculotendon model was adopted in this study. This type of model was considered as the simplest model that adequately represents the fundamental characteristic of single degree-of-freedom joint movement [39]. Although there are three major wrist flexors, they are similar with respect to the fiber type, origin, and anatomical function in terms of wrist flexion-extension [40]. We assume that the lumped model can effectively represent the overall structure of the wrist flexors.

#### 4.3. Individual components and comparison to the NF-method

EC, VC and NC were calculated in the ST group at the same time as the NF-method (at the maximal resistance torque in the fast movement, PIII) to examine whether there were systematic differences in component estimation using the NF-method and the neuromusculoskeletal model. In the control group and STL group, EC was the largest contributor to the total resistant torque, followed by NC. In the STM and STH groups, NC rather than EC was the largest contributor. VC was the smallest contributor for all participants. The increased total resistant torque identified in the participants with stroke was mainly due to the increased NC and EC.

Moderate to very high correlations with the NF-method were found in all three components, with the highest association in NC and the lowest in VC. The moderate correlation in VC was a re-

sult of the inconsistent definitions in the two methods. The viscosity force depends on the velocity and could be related to the shear force from muscle fiber sliding [41]. In the model, VC was therefore defined as a term that is linearly related to the angular velocity. Due to the nature of the NF-method, VC can only be accurately calculated from the force trace before the development of the stretch reflex [13], at the first peak of the fast movement (early viscosity). The late viscosity at PIII was then estimated as 20% of the early viscosity assuming that the velocity was maintained constant [42]. According to our estimation, the late viscosity was 70% (69–72%) of the early viscosity in the ST group. Although further investigation with a larger sample size is needed, the NF-method seems to underestimate the contributions from VC.

#### 4.4. Passive and stretch reflex related parameters

##### 4.4.1. Passive parameters

Compared to the controls, the stiffness was significantly higher in the STM and STH groups due to the increased linear and non-linear exponential terms. As expected, the controls had a very small non-linear coefficient  $k_1$  as the test ROM was far less than their maximal extension angle. Therefore, the passive tissue demonstrated a quasi-linear resistant torque in response to the increased wrist angle. In addition to higher mechanical muscle stiffness  $K_p$  (the linear term), a higher non-linear coefficient  $k_1$  (the exponential term) might indicate a smaller ROM of the wrist joint in the stroke survivors. Shortening of the muscle and/or connective tissues, as is often observed in persons with spasticity, may cause an



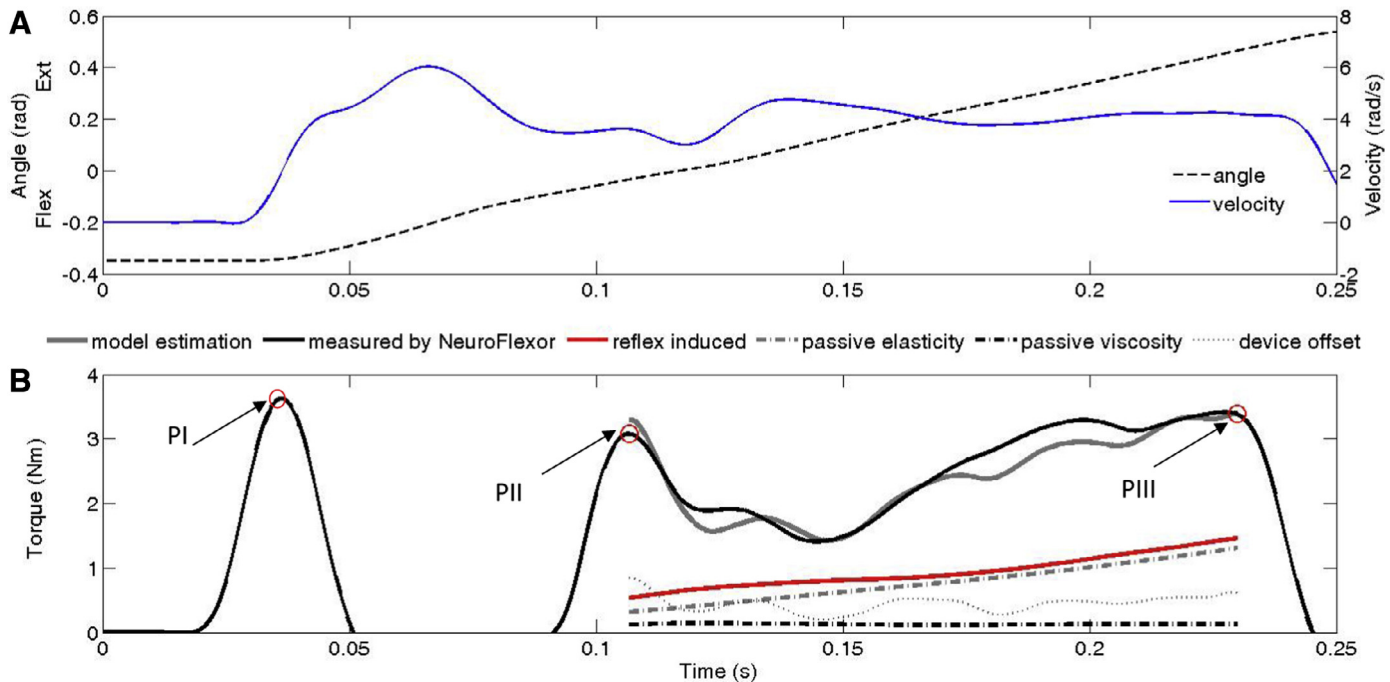


**Fig. 4.** (A) In the fast movement, the wrist joint was passively extended from 20° (0.35 rad) of flexion to 30° (0.52 rad) of extension at 236°/s (4.08 rad/s) using a NeuroFlexor. The black dashed line and black solid line represent the measured joint angle and angular velocity, respectively. (B) A genetic algorithm (GA) was used to estimate stretch reflex-related parameters. The viscosity coefficient,  $B_p$ , estimated from the slow movement was corrected by minimizing the differences between the modeled and measured resistant torque at PI. The optimization was only used to match data recorded in the period of PII to PIII. The contributions from passive (elasticity, viscosity) and stretch reflex-reflected parameters to the resistant torque were specified.

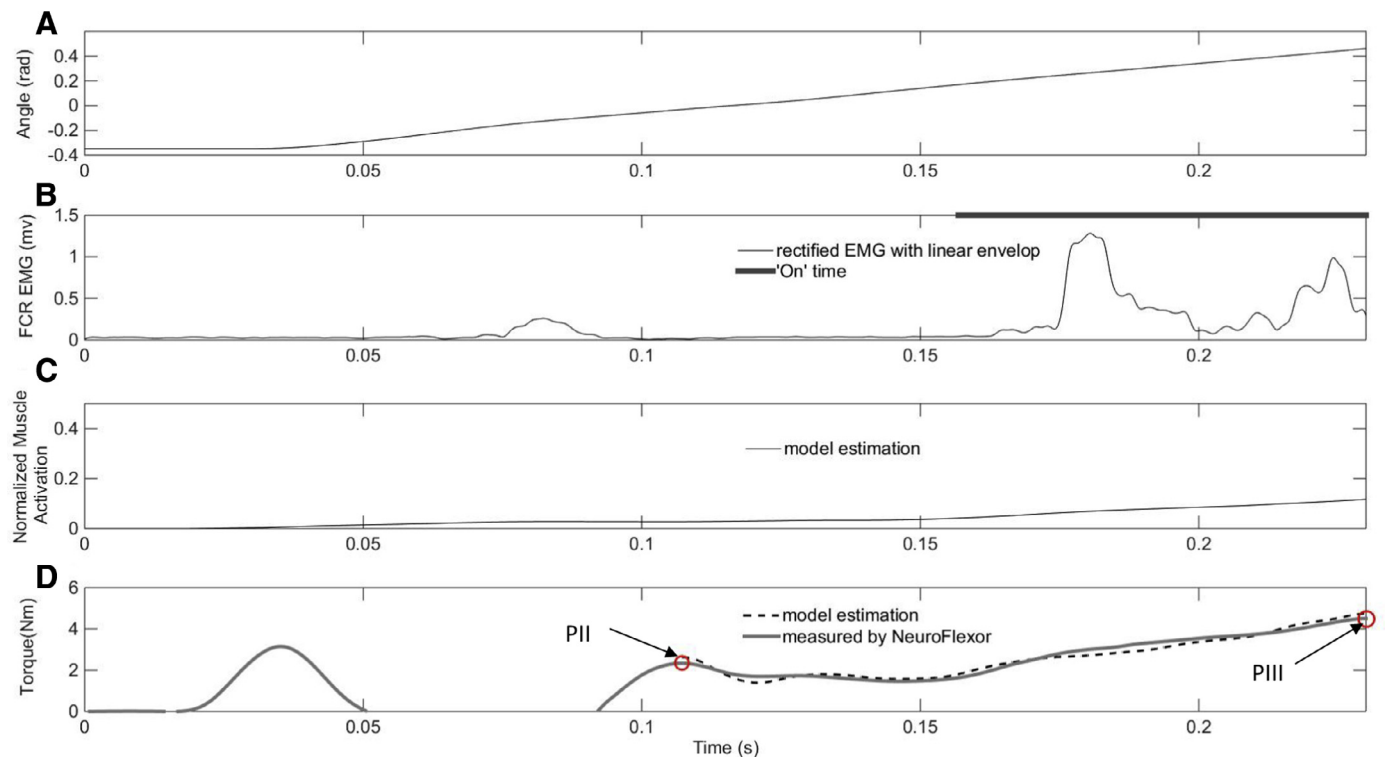


**Fig. 5.** (A) In the fast movement, the wrist joint was passively extended from 20° (0.35 rad) of flexion to 30° (0.52 rad) of extension using NeuroFlexor. (B) The raw EMG recording was sampled at 800 Hz, rectified and linear enveloped with a cutoff frequency of 6 Hz. The FCR was defined as activated when the EMG signal was above a threshold, of three times SD of the baseline EMG. The thick grey line illustrates the activity onset of the FCR, determined in the period of PII to PIII. (C) Model estimated muscle activation induced by wrist extension in the fast movement. (D) Modeled and measured resistant wrist torque showed a good fit during the period of PII to PIII.

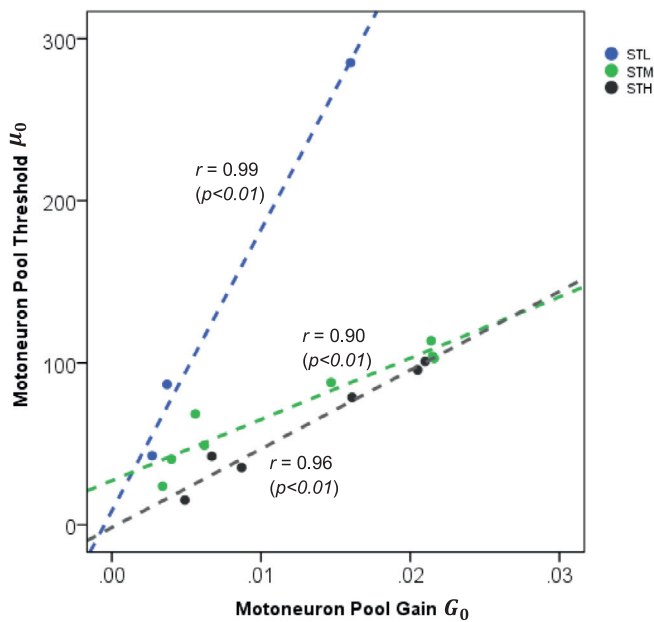


**Fig. 6.** Highly correlated motoneuron pool threshold,  $\mu_0$ , and gain,  $G_0$ , parameters were determined in control (HC), mildly affected (STL), moderately affected (STM) and severely affected (STH) groups. The dash lines represent the linear regression fit to the data.

earlier start of the exponential rise of the stiffness torque. A similar observation was found in a previous study of a stroke population, although the tissue stiffness was modeled differently [43]. In contrast to our findings, a previous NeuroFlexor study reported that increased stiffness occurred in only some participants with

stroke [13]. This inconsistency could be due to a different grade of spasticity in the study cohort. Although the viscosity coefficient  $B_p$  tended to increase with the grade of spasticity, the viscosity generally had a very small contribution to the total resistant torque, especially in the test condition of constant velocity. Due to varying definitions of viscosity in the literature, inconsistent findings in muscle viscosity were reported in persons with stroke with spastic upper limbs [13,43]. The altered viscosity properties in the spastic muscles were considered, to be due to the composition changes in the intra- and extracellular matrix of muscles [44].

#### 4.4.2. Stretch reflex related parameters

The increased NC was further investigated by identifying the motoneuron pool profile for each stroke survivor. Significant differences were observed between the STL and STH groups. In our modeling and analysis, hyperactive reflex was mostly due to lower  $\mu$ . To gain a more meaningful interpretation of each participant's motoneuron pool profile, the threshold  $\mu_0$  (the minimal spindle firing rate) and gain  $G_0$  (the mid-range slope) were defined. Physiologically,  $G_0$  can be interpreted as an intrinsic motoneuron property related to passive membrane properties and the voltage sensitive membrane conductance [21].  $\mu_0$  can be interpreted as the net excitatory and inhibitory inputs to the motoneuron pool. Theoretically, reflex-induced neural excitation can be enhanced by reducing  $\mu_0$  without changing the shape of the profile ( $G_0$ ), i.e., shifting the profile curve to the left. In the participants with stroke,  $\mu_0$  showed a decreasing trend with increased level of spasticity severity, and  $G_0$  demonstrated an opposite tendency. However, between-subgroup differences were not significant for either parameter. Interestingly, we found high correlations between  $\mu_0$  and  $G_0$  in all three subgroups. This finding implied that the abnormal motoneuron pool excitability was possibly modulated through combined effects from the overall synapse input and the intrinsic properties

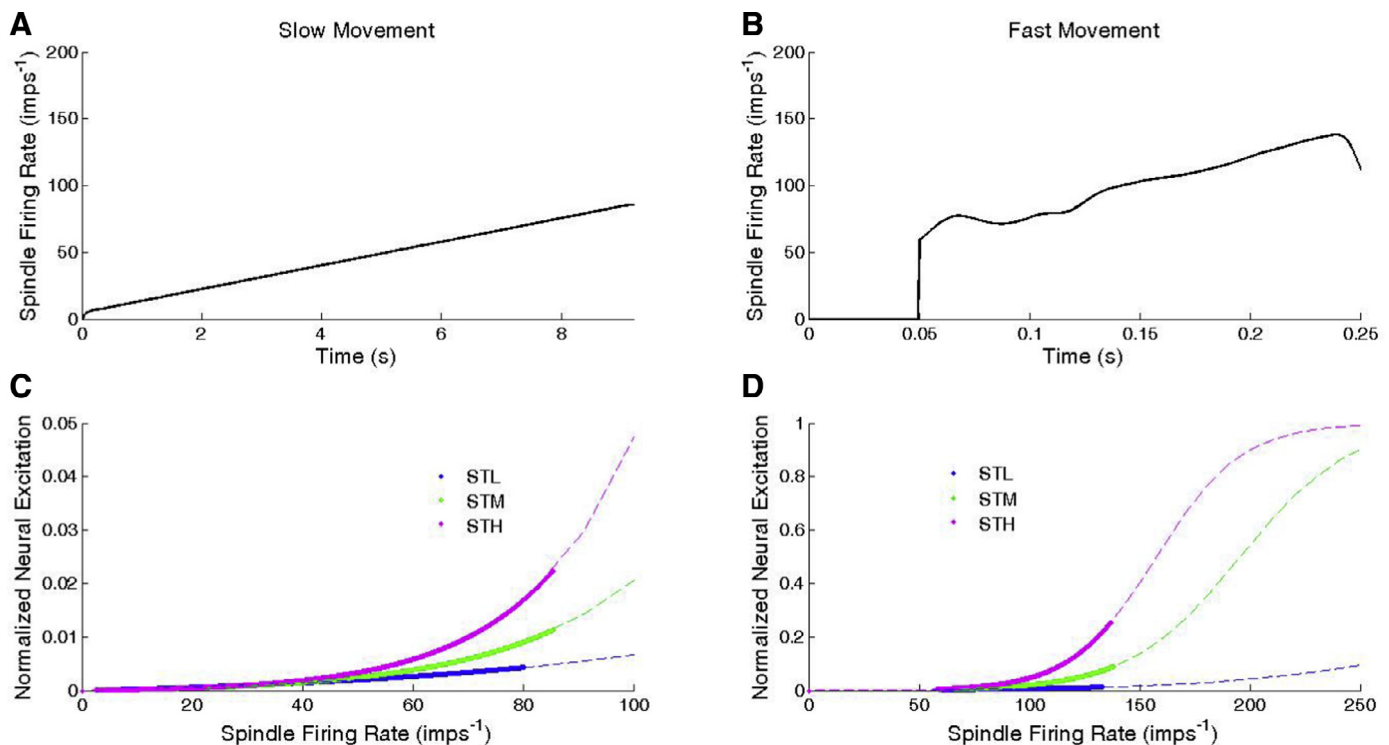


**Fig. 7.** (A)–(B) Model estimated muscle spindle firing rate induced by wrist extension in the slow and fast movement. (C)–(D) Mean motoneuron pool profiles were estimated using optimization in the mildly affected (STL), moderately affected (STM) and severely affected group (STH). The dash lines in magenta, green and blue represent the motoneuron pool profile in the whole range of the spindle firing rate (0–250  $\text{imps}^{-1}$ ) and the solid lines correspond to the range of the neuron excitation estimated in the study. (For interpretation of the references to color in this figure legend, the reader is referred to the web version of this article.)

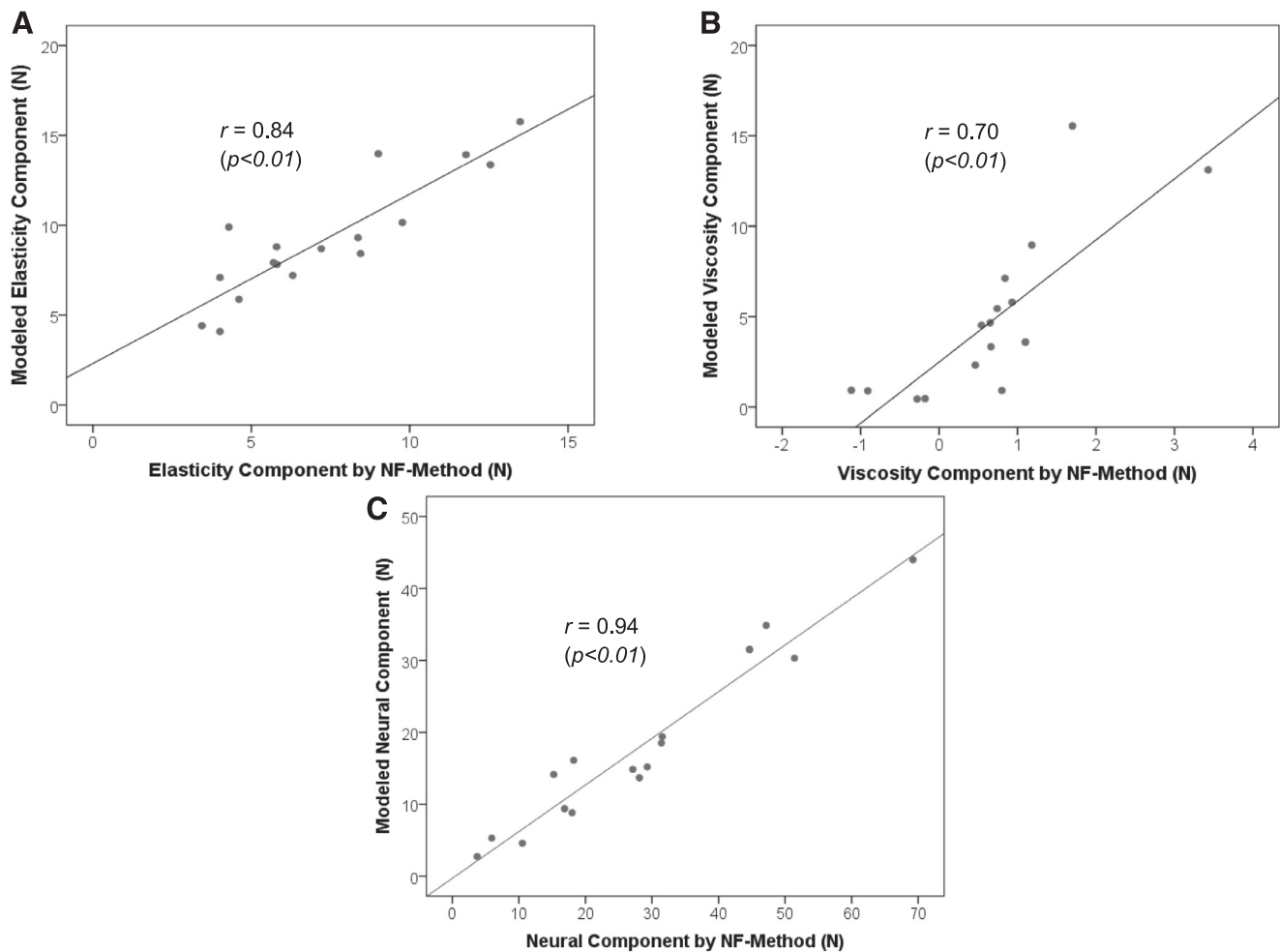


**Fig. 8.** Correlation between components estimated by NF-method and model estimation (A) elasticity component, EC (B) viscosity component, VC, and (C) neural component, NC, in patient groups. The lines represent the linear regression fit to the data.

of motoneurons, such as the conductivity of the motoneuron pool. Although the underlying physiological cause is still not well understood, it is generally accepted that hyperactive stretch reflex is related to changes to the synapse, such as loss in presynaptic inhibition, and changes in the intrinsic properties of the motoneuron, which supports our predictions.

#### 4.5. Limitations

Several simplifications were made in the model. First, it provides a simplified description of the complex interaction of neural control and the musculoskeletal system during movement. Therefore, our goal was to use a general but valid forward neuromusculoskeletal model, that allows for reliable estimation of passive muscle-tendon and stretch reflex related parameters in each person. The validity and sensitivity analysis demonstrated that our model could adequately simulate a passive wrist extension test of spasticity with reasonable computational efficiency. However, we are aware that neurophysiological measurements, such as EMG activity, can provide more information about spasticity when combined with a resistance measurement. In addition, wrist extensors were not included in the model because the EMG signal of the extensors was rarely observed during the test. Second, the non-stretch related background muscle activation was not considered in the model, which could potentially lead to the overestimated NC. A previous study showed that there was non-zero muscle activation

for both the control group and stroke group in the wrist muscles at rest [43]. Future work should take background muscle activation into account. Third, considerable device offset was also noted in the fast movement due to the dynamics of the transmission system of the apparatus, which was not modeled. Nevertheless, we found that the device offset was similar across the participants, which implied a rather minor influence on the model parameter estimation into the context of group comparison. Fourth, the optimization was only performed during part of the fast movement, during which the validated force data were collected. Improvement of the mechanical design of the NeuroFlexor would be valuable in the future. For instance, a modification of extending the wrist joint in the transverse plane could eliminate the gravitational effect of the hand and hand plate. Moreover, the estimation of  $B_p$  also depends on the accuracy of the estimation of the moment of inertia and the angular acceleration of the hand segment, although viscosity has a very small contribution to the total resistant torque.

#### 5. Conclusions

Neural and non-neural related properties of the wrist flexors were estimated in persons with chronic stroke using a forward neuromusculoskeletal model and optimization. The model describes the overall resistance behavior of the wrist joint during the passive extension test of spasticity. The validity of the proposed optimization scheme combining NLS minimization and a



- [10] Blanchette AK, Mullick AA, Moïn-Darbari K, Levin MF. Tonic stretch reflex threshold as a measure of ankle Plantar–Flexor spasticity after stroke. *Phys Ther* 2015.
- [11] Calota A, Feldman A, Levin M. Spasticity measurement based on tonic stretch reflex threshold in stroke using a portable device. *Clin Neurophys* 2008;119:2329–37.
- [12] Ju M, Chen J, Lee H, Lin T, Lin C, Huang Y. Time-course analysis of stretch reflexes in hemiparetic subjects using an on-line spasticity measurement system. *J Electromyogr Kinesiol* 2000;10:1.
- [13] Lindberg P, Gäverth J, Islam M, Fagergren A, Borg J, Forssberg H. Validation of a new biomechanical model to measure muscle tone in spastic muscles. *Neurorehabil Neural Repair* 2011;25:617.
- [14] Gäverth J, Sandgren M, Lindberg P, Forssberg H, Eliasson A. Test-retest and inter-rater reliability of a method to measure wrist and finger spasticity. *J Rehabil Med* 2013;45:630.
- [15] Gäverth J, Eliasson A, Kullander K, Borg J, Lindberg P, Forssberg H. Sensitivity of the NeuroFlexor method to measure change in spasticity after treatment with botulinum toxin A in wrist and finger muscles. *J Rehabil Med* 2014;46:629.
- [16] Katz R, Rymer W. Spastic hypertonia: mechanisms and measurement. *Arch Phys Med Rehabil* 1989;70:144.
- [17] Powers R, Marder-Meyer J, Rymer W. Quantitative relations between hypertonia and stretch reflex threshold in spastic hemiparesis. *Annal Neurol* 1988;23:115.
- [18] Sheean G. The pathophysiology of spasticity. *Eur J Neurol* 2002;9:3–9.
- [19] Dietz V, Sinkjaer T. Spastic movement disorder: impaired reflex function and altered muscle mechanics. *Lancet Neurol* 2007;6:725–33.
- [20] Hidler JM, Rymer WZ. A simulation study of reflex instability in spasticity: origins of clonus. *IEEE Trans Rehabil Eng* 1999;7:327.
- [21] Koo TK, Mak AF. A neuromusculoskeletal model to simulate the constant angular velocity elbow extension test of spasticity. *Med Eng Phys* 2006;28:60.
- [22] de Vlugt E, de Groot JH, Schenkeveld KE, Arendzen JH, van der Helm FC, Meskers CG. The relation between neuromechanical parameters and Ashworth score in stroke patients. *J NeuroEng Rehabil* 2010;7:35.
- [23] van der Krogt H, Klomp A, de Groot JH, de Vlugt E, van der Helm FC, Meskers CG, et al. Comprehensive neuromechanical assessment in stroke patients: reliability and responsiveness of a protocol to measure neural and non-neural wrist properties. *J NeuroEng Rehabil* 2015;12.
- [24] Kim C-S, Eom G-M, Hase K. Modeling and identification of mechanical and reflex properties related to spasticity in stroke patients using multiple pendulum tests. *J Biomech Sci Eng* 2011;6:135–47.
- [25] Winters J, Stark L. Analysis of fundamental human movement patterns through the use of in-depth antagonistic muscle models. *IEEE Trans Biomed Eng* 1985;32:826.
- [26] Robertson G, Caldwell G, Hamill J, Kamen G, Whittlesey S. Research methods in biomechanics. 2nd ed. Human Kinetics; 2013.
- [27] Prochazka A, Gorassini M. Models of ensemble firing of muscle spindle afferents recorded during normal locomotion in cats. *J Physiol* 1998;507:277.
- [28] Wilson L, Gandevia S, Inglis J, Gracies J, Burke D. Muscle spindle activity in the affected upper limb after a unilateral stroke. *Brain J Neurol* 1999;122:2079.
- [29] Fuglevand A, Winter D, Patla A. Models of recruitment and rate coding organization in motor-unit pools. *J Neurophys* 1993;70:2470.
- [30] Thelen DG. Adjustment of muscle mechanics model parameters to simulate dynamic contractions in older adults. *J Biomech Eng* 2003;125:70–7.
- [31] Goldberg DE. Genetic algorithms in search, optimization, and machine learning 1989 1989.
- [32] Macefield V. Discharge rates and discharge variability of muscle spindle afferents in human chronic spinal cord injury. *Clin Neurophys* 2013;124:114.
- [33] Wang R, Gutierrez-Farewik E. Compensatory strategies in response to excessive muscle co-contraction at the ankle joint during walking. *Gait Posture* 2014;39:926–32.
- [34] De Serres S, Milner T. Wrist muscle activation patterns and stiffness associated with stable and unstable mechanical loads. *Exper Brain Res* 1991;86:451.
- [35] Gielen C, Houk J. Nonlinear viscosity of human wrist. *J Neurophys* 1984;52:553.
- [36] Fukushima S, Komi P, Järvinen M, Miyashita M. Comparison between the directly measured Achilles tendon force and the tendon force calculated from the ankle joint moment during vertical jumps. *Clin Biomech* 1993;8:25–30.
- [37] Heckman C, Binder MD. Computer simulation of the steady-state input–output function of the cat medial gastrocnemius motoneuron pool. *J Neurophysiol* 1991;65:952–67.
- [38] Niu CM, Nandyala SK, Sanger TD. Emulated muscle spindle and spiking afferents validates VLSI neuromorphic hardware as a testbed for sensorimotor function and disease. *Front Comput Neurosci* 2014;8.
- [39] Winters J, Bagley A. Biomechanical modeling of muscle–joint systems. *IEEE Eng Med Biol Mag* 1987;6:17.
- [40] Hamill J, Knutzen KM. Biomechanical basis of human movement Lippincott Williams & Wilkins; 2006.
- [41] Bagni M, Cecchi G, Colomo F, Garzella P. Absence of mechanical evidence for attached weakly binding cross-bridges in frog relaxed muscle fibres. *J Physiol* 1995;482:391.
- [42] Halar E, Stolov W, Venkatesh B, Brozovich F, Harley J. Gastrocnemius muscle belly and tendon length in stroke patients and able-bodied persons. *Arch Phys Med Rehabil* 1978;59:476.
- [43] Helgadottir A. Identification of muscle activation at rest Master thesis. Delft University of Technology; 2013.
- [44] Lieber R, Runesson E, Einarsson F, Fridén J. Inferior mechanical properties of spastic muscle bundles due to hypertrophic but compromised extracellular matrix material. *Muscle Nerve* 2003;28:464.